2023

Structural and Solution Speciation Studies on Selected [Cu(NN)(OO)] Complexes and an Investigation of their Biomimetic Activity, ROS Generation and their Cytotoxicity in Normoxic, Hypoxic and Anoxic Environments in MCF-7 Breast Cancer-Derived Cells

Hollie Jenkins
Technological Universit Dublin, Tallaght, Ireland, helen.jenkins@tudublin.ie

Funder: Science Foundation Ireland –Investigator Programme SFI/12/IP/1390; Irish Reseach Council Postgraduate Awards (EM 200701); Centre of Applied Science for Health, TU Dublin; D24 FKT9; National Research, Development and Innovation Office (Hungary) TKP-2021-EGA-32 and by the “Lendület” Programme (ELKH, LP2019-6/2019) (EAE); K124544; FAPERJ (Edital N.° 43/2013, Programa de Apoio ao Doutorado-Sanduíche Reverso), CNPq and CAPES fundings; Programme for Research in Third Level Institutions (PRTLI) Cycle 5 under the supervision of Dr. Úna Prendergast; European Regional Development Fund (ERDF)

Journal of Inorganic Biochemistry 249 (2023) 112383

Contents lists available at ScienceDirect

Journal of Inorganic Biochemistry

journal homepage: www.elsevier.com/locate/jinorgbio

Structural and solution speciation studies on selected [Cu(NN)(OO)] complexes and an investigation of their biomimetic activity, ROS generation and their cytotoxicity in normoxic, hypoxic and anoxic environments in MCF-7 breast cancer-derived cells

Hollie Jenkins [a], Louise MacLean [a], Siobhán McClean [b], Gordon Cooke [a,h], Michael Devereux [c], Orla Howe [c,d], Marcos D. Pereira [e,i], Nóra V. May [f], Éva A. Enyedy [g], Bernadette S. Creaven [a,h,*]

[a] Centre of Applied Science for Health, TU Dublin, Tallaght Campus, D24 FKT9, Ireland
[b] School of Biomolecular and Biomedical Science, University College Dublin, Belfield Dublin 4, Ireland
[c] Centre for Biomimetic and Therapeutic Research, Focas Research Institute, TU Dublin, Camden Row, Dublin 8, Ireland
[d] School of Biological, Health and Sport Sciences, TU Dublin, City Campus, D07 XT95, Ireland
[e] Departamento de Bioquímica, Instituto de Química, Universidade Federal do Rio de Janeiro, Brazil
[f] Centre for Structural Sciences, Research Centre for Natural Sciences, Magyar tudósok körútja 2, Budapest H-1117, Hungary
[g] Departmen of Molecular and Analytical Chemistry, Interdisciplinary Excellence Centre and MTA-SZTE Lendület Functional Metal Complexes Research Group, University of Szeged, Dóm tér 7, Szeged H-6720, Hungary
[h] School of Chemical and BioPharmaceutical Sciences, Technological University Dublin, Central Quad Building, Grangegorman, Dublin D07 ADY7, Ireland
[i] Rede de Micrologia – FAPERJ, Rio de Janeiro, Brazil

ARTICLE INFO

Keywords:
Copper(II) complexes
Cancer
Hypoxia
Reactive oxygen species
Speciation

ABSTRACT

Reactive oxygen species(ROS) generation with subsequent DNA damage is one of the principle mechanisms of action assigned to copper-based anticancer complexes. The efficacy of this type of chemotherapeutic may be reduced in the low oxygen environment of tumours. In this study the cytotoxicity of three complexes, [Cu(dips)(phen)] (**1**), [Cu(ph)(phen)]·2H_2O (**2**) and [Cu(ph)(bpy)]·H_2O (**3**) (disp: 3,5-diisopropylsalicylate, phen: 1,10-phenanthroline, ph: phthalate, bpy: 2,2′-bipyridyl) were assessed for anticancer activity in the breast-cancer derived MCF-7 line under normoxic, hypoxic and anoxic conditions. In an immortalised keratinocyte HaCaT cell line, the cytotoxicity of complexes **2** and **3** was significantly reduced under both normoxic and hypoxic conditions, whilst the cytotoxicity of complex **1** was increased under hypoxic conditions. The ability of the complexes to generate ROS in the MCF-7 cell line was evaluated as was their ability to act as superoxide dismutase(SOD) and catalase mimics using a yeast cell assay. ROS generation was significant for complexes **2** and **3**, less so for complex **1** though all three complexes had SOD mimetic ability. Given the ternary nature of the complexes, solution speciation studies were undertaken but were only successful for complex **3**, due to solubility issues with the other two complexes. The concentration distribution of various species, formed in aqueous solution, was evaluated as a function of pH and confirmed that complex **3** is the dominant species at physiological pH in the mM concentration range. However, as its concentration diminishes, it experiences a progressive dissociation, leading to the formation of binary complexes of bpy alongside unbound phthalate.

Abbreviations: bpy, 2,2′-bipyridyl; CAT, catalase; DCF, 2′,7′-dichlorofluorescein; DCM, dichloromethane; DMSO, dimethyl sulfoxide; EDTA, ethylenediaminetetraacetic acid; EtOH, ethanol; H_2DCFDA, 2′,7′-dichlorodihydrofluorescein diacetate; HPCINOL, 1-[bis(pyridine-2-ylmethyl)amino]-3-chloro-propan-2-ol; MEM, minimum essential *medium*; MTT, methylthiazolyldiphenyltetrazolium bromide; NBT, nitro blue tetrazolium; PBS, phosphate-buffered saline; ph, phthalate; phen, 1,10-phenanthroline; ROS, reactive oxygen species; SEM, standard error of the mean; SOD, superoxide dismutase; TBHP, tert-butyl hydroperoxide; YPD, yeast extract–peptone–dextrose.

* Corresponding author at: Centre of Applied Science for Health, TU Dublin, Tallaght Campus, D24 FKT9, Ireland.
E-mail address: bernie.creaven@tudublin.ie (B.S. Creaven).

https://doi.org/10.1016/j.jinorgbio.2023.112383
Received 8 June 2023; Received in revised form 8 September 2023; Accepted 18 September 2023
Available online 22 September 2023

1. Introduction

Breast cancer is the most common cancer, with 2.26 million people diagnosed globally in 2021. 24.2% of all cancers diagnosed in women are breast cancer, which has the highest mortality of any cancer in women worldwide and particularly in European women compared to other cancer types [1,2]. The development of new drug therapies and combinations of therapies for early-stage and locally advanced breast cancer is urgently needed [3–5]. Chemotherapeutic systemic therapies are still widely used particularly as adjuvant chemotherapy after surgery to stop the spread of the disease. Current breast cancer chemotherapeutics such as Doxorubicin, Cisplatin and Paclitaxel, involve DNA interaction and/or disruption of cellular pathways with subsequent or concomitant generation of reactive oxygen species (ROS) [3]. Normal cellular metabolism also leads to generation of ROS and it is well accepted that controlled levels of ROS are required for several cellular functions in healthy cells, including cellular signalling pathways and gene expression. Paradoxically, ROS concentrations are high in many cancer cells and further elevated by chemotherapy, triggering cell death via apoptosis [6,7]. ROS also act as signalling molecules within cancer cells, inducing angiogenesis and consequent metastasis. In Neoadjuvant therapy with doxorubicin and paclitaxel prior to surgery promoted metastases in the mice bearing human breast tumours [8]. Given that an estimated 90% of breast cancer deaths are the result of metastases (mainly to liver, brain, lungs and bone) [7–9], using treatments that generate ROS are not without concern [10–12]. ROS are known to have a controversial role during cancer initiation and progression and although several studies have tried to manipulate intracellular ROS levels using antioxidants or pro-oxidation agents, it is not yet clear how to safely target oxidation for cancer therapy [13].

Oxidative damage from ROS can arise from the Fenton reaction, whereby intracellular reductants can reduce Cu(II) complexes to Cu(I), followed by Cu(I) reactions with hydrogen peroxide, generating hydroxyl radicals and hydroxide anion [14,15]. Harnessing that reaction to develop copper-based chemotherapeutics has been ongoing for decades since the discovery of the nucleolytic activity of bis(1,10-phenanthroline)copper(II) $[Cu(phen)_2]^{2+}$ towards dsDNA [16], in the presence of O_2 and a reducing agent. Since then extensive investigations into related copper phen and similar NN donor ligands have been undertaken as recently reviewed [17]. One series of copper(II) complexes from a series called Casiopeinas are under intense investigation for their mode of action, and two of the series are currently in Phase I clinical trials [18]. Two of the three complexes (**1**–**3**) studied in this work (Fig. 1) were previously assessed for their ability generate ROS in SK-OV-3 cancer cells [19]. ROS generation was greater for complex **2** relative to complex **3** and correlated with their relative cytotoxicity, and their ability to, bind to, and cleave DNA [20,21].

DNA-damaging ROS are typically produced via redox active metal centres in the presence of external agents like H_2O_2, mercaptopropionic acid or light [22,23]. Copper(II) polypryidyl complexes have been investigated as superoxide dismutase mimics as this enzyme coverts superoxide to hydrogen peroxide. A copper(II) complex which can act as a superoxide dismutase (SOD) mimic, and undergoing Fenton chemistry in the presence of cellular reductants should have an enhanced ability to act as a DNA nuclease and hence chemotherapeutic agent. In some cases these same copper(II) polypyridyl complexes have shown catalase (CAT) mimetic ability and could potentially act as detoxifying agents **as** CAT converts hydrogen peroxide to water and oxygen reducing oxidative stress [24,25]. However, concerns have been raised recently by our and other groups with using cell-free models for assessment of biomimetic activity by copper complexes [26,27], so in this study complexes **1–3** were assessed for their ability to act as SOD and CAT mimetics using a *Saccharomyces cerevisiae* model to gain better insights into the role of the complexes in ROS production/amelioration and establish a possible relationship between that activity and their cytotoxicity [28].

One consideration in using ROS generation as a strategy to treat tumours is that tumours exhibit heterogeneity as oxygen is depleted, posing a challenge to the treatment of solid tumours [29]. Heterogeneity alters cell morphology, gene expression, motility, angiogenesis, immunogenic and metastatic possibilities, dramatically affecting their growth, treatment and mortality [30,31]. This is exploited whereby drugs with nitro substituents, transition metals and/or aromatic-N-oxide substituents have potential as pro-drugs that can differentiate between hypoxic and normoxic cells [32,33]. Strese et al., [34] showed cell survival in response to Tirapazamine was greatest in hypoxic > anoxic > normoxic conditions. However, Cisplatin and Mitomycin C were far less sensitive to oxygen conditions with little change in cell survival under a range of oxygen conditions. Chemotherapeutic compounds which rely on the generation of ROS to induce apoptosis in cancer cells are less effective in hypoxic environments and consequently this study probed the cytotoxicities of complexes **1**–**3** under varying oxygen conditions, relative to Cisplatin, Doxorubicin and Mitoxantrone, in breast cancer-derived MCF-7 cells. The cytotoxicity of the three complexes was also screened using an immortalised keratinocyte HaCaT cell line in both normoxic and hypoxic conditions.

The ternary nature of the three complexes studied here also prompted speciation studies. The concentration distribution of various species, formed in aqueous solution, was also evaluated as a function of pH and in one study in 2020 [35], in which copper(II) ternary complexes of bipyridine and amino acids were investigated, the *bis*-ligand bipy complex of copper(II) was found to dominate at physiological pH. Herein, the solution speciation studies for complex **3** are reported, together with the single crystal structure of complex **1**. Solution equilibria determination yields important thermodynamic information regarding complex formation, complex stability and ligand affinity for a metal ion in solution [26,36], and such studies are an effective method in determining the speciation of metal complexes in solution in controlled conditions [37,38].

The relationship between the biomimetic activity of the three complexes, ROS generation specifically in the MCF-7 breast cancer cell line,

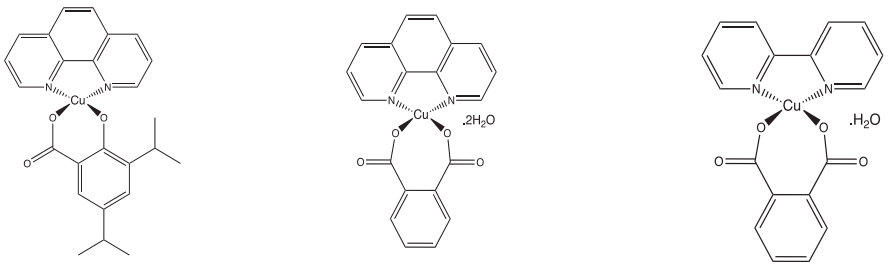

Fig. 1. Structures of copper(II) complexes **1–3** (disp: 3,5-diisopropylsalicylate, phen: 1,10- phenanthroline, ph: phthalate, bpy: 2,2′-bipyridyl).

and their in vitro cytotoxicity under normoxic, hypoxic and anoxic conditions is reported. In addition, we continued our studies on speciation of copper complexes at physiological pH to elucidate the likely active form of the complexes in cell-based studies.

2. Results and discussion

2.1. Structural studies

Complexes **1**–**3** were synthesized according to previously published procedures (details in supplementary Information) [19,24,39]. Green crystals of complex **1**, were isolated through the dissolution of its green powder form in hexane, and subsequent diffusion into dichloromethane (DCM). Analysis of the diffraction pattern resulted in the proposed crystal structure of catena-((μ$_2$–3,5-diisopropylsalicylato-O,O′,O″)-(1,10-phenantroline-N,N′)-copper(II)), Fig. 2a. Crystal data and structure refinement parameters are collected in Table S1. The complex crystallized in a monoclinic crystal system of space group *C2/c*. The complex was found to be a one-dimensional polymer chain, with both carboxylic oxygens from one salicylate ligand bridging across two copper centres, with one oxygen in the equatorial position while the other is in the axial position. The phenolic oxygen is also bound to copper, and both nitrogen atoms of the phenanthroline ligand are coordinated in the same plane. The coordination mode surrounding the copper centre is O, O,O,N,N, and as a penta-coordinated species, the bond angles, (Table S2, supplemental information), are indicative of a distorted square pyramidal geometry. The bond angles between the equatorial bound ligands are 90.7° (O2-Cu-N2), 91.6° (O3-Cu-N1), 95.2° (O3-Cu-O2) and 80.4° (N2-Cu-N1), showing the N-Cu-N angle to be slightly compressed relative to the 90° angle expected in a square planar-type geometry, while the O-Cu-O angle is slightly expanded. The angles between the axial bound oxygen (O1) and equatorial donor atoms (N1, N2, O2 and O3) deviate from the expected 90°, while the atoms trans to each across the plane are considerably less than the expected 180° angle. As the axial position beneath the plane is empty, and there are four coordinated atoms in one plane, the geometry can be described as distorted square pyramidal. The structure is consistent with the assigned IR spectra (see data in the supplemental information), where $\Delta_{OCO} < 200$ cm^{-1} is indicative of bidentate binding, and in complex **1** the Δ_{OCO} value was found to be 158 cm^{-1}. The bond lengths observed for the each of the equatorial nitrogen atoms bound to the central copper ion are within 0.006 Å of one another, as are those of the equatorial oxygens (within 0.03 Å). The equatorial Cu—O bonds are shortest, as expected, as negatively charged ligands form shorter metal to ligand bonds. The axial Cu—O1 bond is the longest, which is consistent with bond lengths observed in other copper(II) complexes of similar donor atoms and geometry [24,40,41].

The coordination of complex **1** forms a one-dimensional polymer chain in solid phase, Fig. 2b. The copper centres are twisted at an angle of 78.45° between their equatorial planes, while the equatorial angle between the aromatic rings of the diisopropylsalicylate and 1,10-phenanthroline is 26.31°, Fig. S1. Hydrogen bonding is apparent between the oxygens and the alkyl hydrogens, Table S3, which along with π-π stacking interactions between the aromatic regions of the phen ligands, stabilises the crystal structure, as shown in Fig. S2. No interaction was observed between the diisopropylsalicylate groups. Within the 1D polymer of complex **1**, columns are formed in the crystallographic direction of *b*, with the intermolecular H-bonding and π-π interactions cause a driving force in the *c* direction and diisopropylsalicylate are facing one another in direction of *a*, as shown in Fig. S3a. The packing arrangements viewed from the three crystallographic directions are shown in Fig. S3b. Complexes containing salicylate-derived ligands more commonly form cyclic dimer systems, however for complex **1**, a 1D polymer were observed, perhaps due to the steric hindrance of two bulky diisopropylsalicylate groups. The crystal structure of **3** has been previously reported and the geometry around the copper(II) centre also reported as distorted square pyramidal [42].

2.2. Proton dissociation processes of the ligands and their copper(II) complexation for complex *3*

Solution studies of all three complexes were attempted for this work but the poor solubility of complexes **1** and **2** in the applied medium made them unmeasurable using these analytical methods. Due to the insufficient water solubility of the ternary Cu(II) – phthalate (A) – bpy (B) complexes the pH-potentiometric titrations were performed in a 30% (*v*/v) dimethyl sulfoxide (DMSO)/H_2O solvent mixture (instead of water). However, the pK_a values of the ligands and the stability constants of their binary Cu(II) complexes were already reported in the literature in aqueous solution [43]. Herein the data for the binary systems have been also determined in the presence of the 30% DMSO as they are needed for the computation of the stability constants for the formation of the ternary complexes under the same condition. pK_a values of these ligands and overall stability constants (β) of the binary and ternary Cu(II) complexes obtained by pH-potentiometry furnishing the best fits to the experimental data are listed in Table 1. The speciation

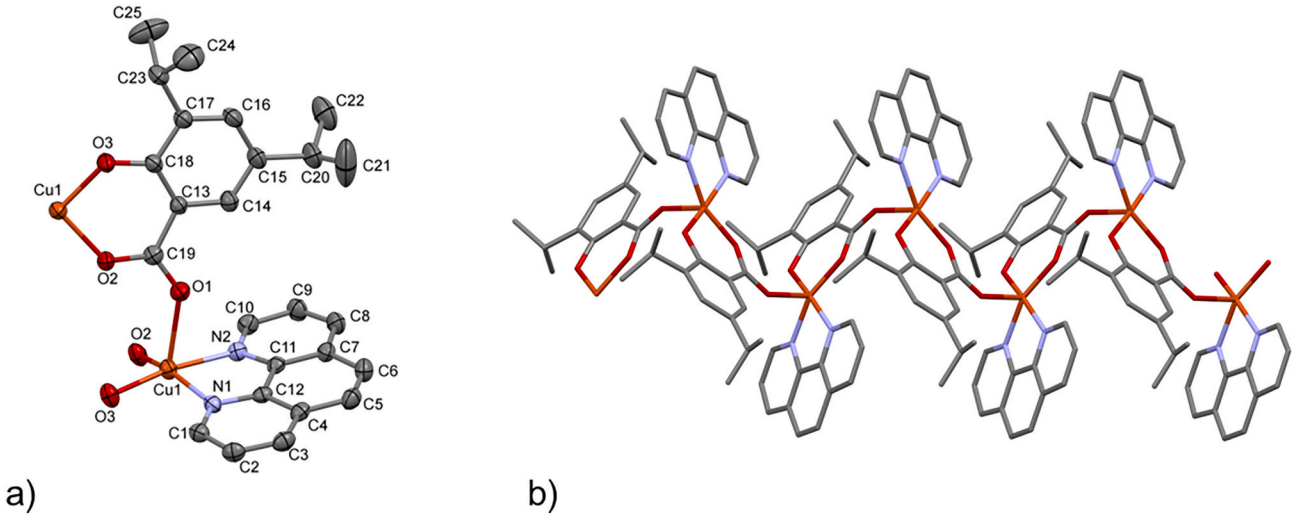

Fig. 2. a) Molecular crystal structure of complex **1**, catena-((μ$_2$–3,5-diisopropylsalicylato-O,O′,O″)-(1,10-phenantroline-N,N′)-copper(II)) with hydrogens omitted for clarity and b) one-dimensional polymer chain in the crystal of complex **1.** Displacement parameters are drawn at 30% probability level.

Table 1
Proton dissociation constants (pK_a) of the ligands and overall stability constants (logβ) of the complexes formed in the binary and ternary systems of Cu(II) - phthalate (A^{2-}) - 2,2′-bipyridine (B) determined by pH-potentiometry, UV–visible spectrophotometry and EPR {30% (*v*/v) DMSO/H_2O; t = 25 °C, I = 0.10 M (KCl)}.

	30% DMSO/H_2O pH-potentiometry	30% DMSO/H_2O EPR	H_2O pH-potentiometry
pK_1 (H_2A)	3.33 ± 0.04	–	3.03[c]
pK_1 (HA^-)	5.87 ± 0.02	–	5.60[c]
logβ [CuA]	4.44 ± 0.03	–	3.49[d]
logβ $[CuA_2]^{2-}$	7.37 ± 0.09	–	6.08[d]
pK_1 (HB)	3.95 ± 0.03	–	4.64[e]
logβ $[CuB]^{2+}$	≥8.5[a]	≥8.5[b]	9.06[e]
logβ $[CuB_2]^{2+}$	13.76 ± 0.04	14.14 ± 0.06	14.96[e]
logβ $[CuB_3]^{2+}$	17.42 ± 0.05	16.7 ± 0.1	18.21[e]
logβ $[Cu_2B_2H_{-2}]^{2+}$	6.63 ± 0.05	6.0 ± 0.5	7.27[e]
logβ $[CuBH_{-2}]$	−9.03 ± 0.04	−9.98 ± 0.03	−9.10[e]
logβ $[CuB_2H_{-1}]^+$	5.19 ± 0.05	4.64 ± 0.03	5.38[e]
logβ $[CuBH_{-1}]^+$	–	−0.50 ± 0.08	–
logβ $[Cu_2B_4{-1}]$	–	–	23.46
logβ [CuAB]	12.83 ± 0.03 12.74 ± 0.03[a]		–

[a] Determined by UV–visible spectrophotometric titrations.
[b] Estimated from the UV–visible spectra recorded in the pH range 1–2 using individual samples in which the KCl content was partly or completely exchanged by HCl to keep I constant (0.10 M).
[c] Data taken from Ref. [A. Misra, S. Mital, G.K. Chaturvedi, J. Indian Chem. Soc. 57 (1980) 42–45.].
[d] Data taken from Ref. [G.V. Narayana, S.J. Swamy, P. Lingaiah, Indian J. Chem. 27 A (1988) 613–616.].
[e] Determined by the combination of pH-potentiometry and UV–visible spectrophotometry. Data taken from Ref. [I. Fábián, Inorg. Chem. 28 (1989) 3805–3807.].

study was completed by UV–visible (UV–vis) spectrophotometric titrations and electron paramagnetic resonance (EPR) spectroscopic measurements (vide infra for detailed information). As it is expected the pK_a values of phthalic acid are higher, while that of bpy is lower in the presence of DMSO compared to the data reported in aqueous solution due to the better solvation of the neutral ligand forms in the more apolar solvent compared to the aqueous phase. Namely, the pK_a of cationic acids is such as bpy (HB^+) diminished, while that of the acids resulting in anionic bases such as phthalic acid (HA^-, A^{2-}) is increased in the presence of DMSO compared to pure water due to the isoelectronic and charge neutralization protonation processes, respectively.

Phthalic acid forms [CuA] and $[CuA_2]^{2-}$ complexes with Cu(II) with relatively low stability. The ligand could not protect the metal ion against the hydrolysis and precipitate appeared in the solution at pH > 6.5, data collected bellow this pH were used for the calculations (Table 1).

Bpy forms much higher stability complexes with Cu(II) compared to phthalate: the coordination of the ligand starts already at pH < 2, the overall formation constant of the mono-ligand complex $[CuB]^{2+}$ formed at low pH was determined by UV–visible spectrophotometry on individual samples following the changes of the d-d bands, where KCl was partially or completely replaced by HCl in order to adjust the pH and keep the ionic strength constant. By fitting the spectra recorded between pH 1.0 and 3.0 the stability constants for $[CuB]^{2+}$ could be calculated. After keeping it constant, the logβ values of the other complexes (see Table 1) were calculated for the data obtained by pH-potentiometric titrations. The complexes with −1 or − 2 stoichiometric numbers for the hydrogen (H_{-1} or H_{-2}) are regarded as mixed hydroxido complexes. The speciation model was completed based on the findings obtained by EPR spectroscopy (section 2.3.2).

Then the Cu(II) - A - B ternary system was studied by pH-potentiometric titrations at 1:1:1, 1:2:1 and 1:1:2 ratios and overall stability constant for the complex [CuAB] was determined (Table 1). UV–visible titrations were also performed providing a very similar stability constant (Table 1). Based on the determined constant the formation of the ternary species [CuAB] is excepted at 1:1 metal-to-bpy ratio in the presence of 1 or 2 equivalents of the phthalic acid, while at the two equivalents of the bpy its formation is less favorable. It was confirmed by the UV–visible titrations data (Fig. 3), namely the spectra recorded at the 1:1:2 (Cu:A:B) ratio showed strong similarity to those obtained for the Cu(II) - bpy (1:2) binary system; whereas the spectra recoded at 1:1:1, 1:2:1 (Cu:A:B) ratios clearly showed the formation of a novel type species at pH 4–9 with a λ_{max} ~ 645 nm. The addition of 1 equivalent of phthalic acid to the Cu(II)-bpy (1:1) system resulted in significant differences in this pH range concerning the λ_{max} and absorbance values at e.g. 660 nm, which confirms the formation of the ternary complex (Fig. 4). The UV–vis spectra were deconvoluted and the individual molar absorbance spectra of the various species were computed and λ_{max} = 646 nm was obtained for [CuAB]. For [CuAB] complex with the (O,O) (N,N) coordination mode the λ_{max} is expected to be 698 nm based on the empirical formula defined by Sigel and Martin [44] and improved by Prenesti et al. [45–48], which originally correlates the λ_{max} of the d–d band of the Cu(II) ion with the character of coordinating ligands for pure equatorially coordinated complexes [44]. (Coefficients 0.353 and 0.363 were used for the carboxylate oxygens and the piridinyl nitrogens, respectively [47,48]). The mean value (728 nm) of the λ_{max} of $[CuA_2]^{2-}$ (707 nm) and $[CuB_2]^{2+}$ (748 nm) could not be used for comparison. The reason is that in $[CuB_2]^{2+}$ only two nitrogens were reported to be in the planar environment resulting in a red shift compared to the case when all the four nitrogens are assumed to be in the equatorial plane (689 nm) [47]. The experimentally obtained value of [CuAB] is significantly blue-shifted from the calculated one (by 52 nm (698–646 nm)) as a possible consequence of the non-regular square planar geometry (see section 2.3.3). The axial coordination of the donor atoms would result in a red shift [47].

The relative stability of the mixed-ligand complex [CuAB] can be evaluated via the calculation of the stability constant expected on a statistical consideration:

$$\log\beta\,[CuAB]^{stat} = ½\,\log\beta\,[CuA_2] + ½\,\log\beta\,[CuB_2] + \log 2.$$

The value logβ $[CuAB]^{stat}$ is 10.73, which is somewhat lower compared with the experimentally determined constant, thus the formation of this species is rather favorable. However, on the basis of the computed concentration distribution curves (Fig. 4), it can also concluded that at physiological pH the original mixed-ligand complex (complex **3**, [CuAB]) undergoes some extent of dissociation leading to the formation of the binary $[CuB]^{2+}$ and $[Cu_2B_2(OH)_2]^{2+}$, and the phthalate ligand is partly released.

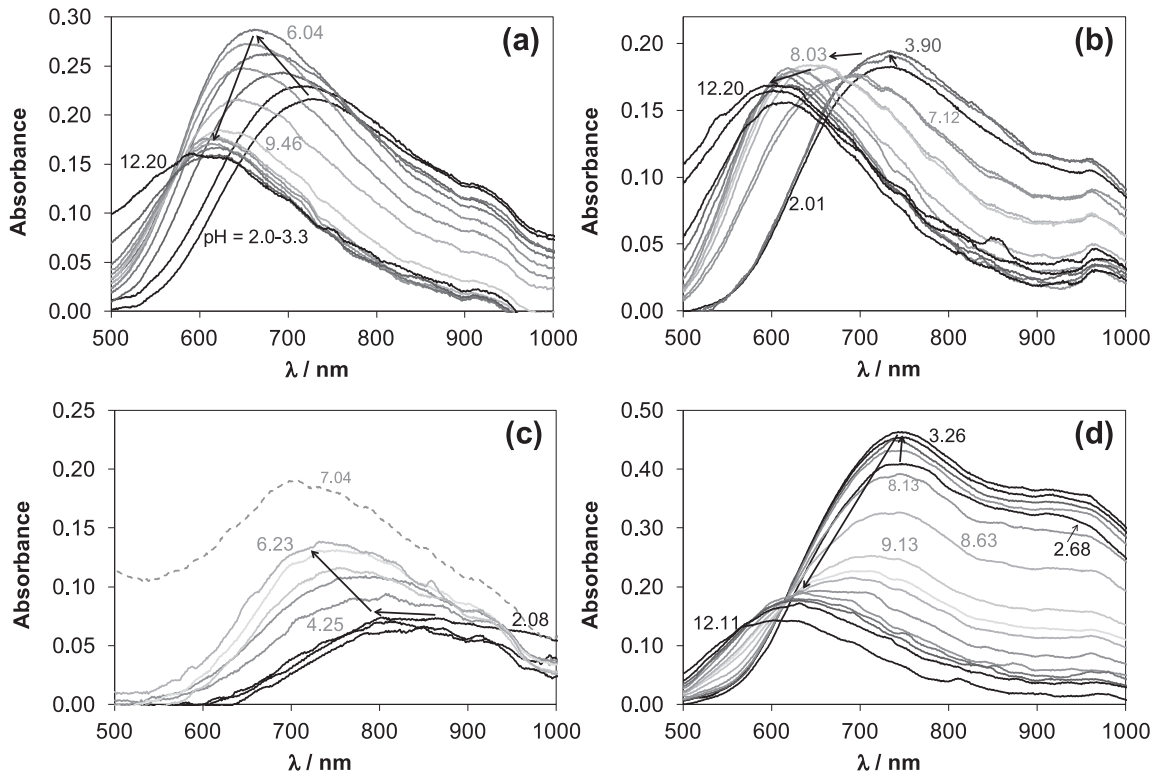

Fig. 3. UV–visible spectra recorded at various pH values of Cu(II) - phthalate (A^{2-}) - bpy (B) (1:1:1) ternary (a); Cu(II) - B (1:1) binary (b), Cu(II) - A (1:1) binary (c) and Cu(II) - B (1:2) binary (d) systems. {30% (v/v) DMSO/H_2O; t = 25 °C, I = 0.10 M (KCl); $c_{Cu(II)}$ = 2 mM; l = 2 cm}.

2.3. EPR spectroscopic studies

2.3.1. Copper(II)-phthalic acid equilibrium system

In the solution containing copper(II) and phthalic acid the formation of [CuA] was detected above pH ~ 3 and at three-fold ligand excess the bis complex [CuA_2] formed at pH > ~6 (Fig. S4). Above pH ~7 both in equimolar solution and ligand excess the disappearance of the EPR signal was observed therefore, the alkaline region was not investigated (similarly to the pH-potentiometric studies). The anisotropic EPR spectra of [CuA] showed a rhombic g-tensor with well resolved perpendicular copper hyperfine couplings (Fig. S5). Square planar geometry with the coordination of water molecules in the open equatorial or axial coordination positions can be suggested for this complex. When the equatorial water molecules are replaced by a second phthalic acid in [CuA_2] the ligand field changed only slightly (Table 1). In solid phase an elongated octahedral geometry of the [$CuA_2(H_2O)_2$] was found in a coordination polymer where the carboxylate oxygen plays a bridging role between neighbouring copper centres (Scheme S5) [49]. Such polymerization was not detected under our measuring conditions.

2.3.2. Copper(II) - bipyridine equilibrium system

The copper(II) – bpy equilibrium system was studied by EPR spectroscopy. EPR spectra were recorded in 30% DMSO/water solution at room temperature (298 K) and in frozen solution (77 K) at different metal-to-ligand concentration ratios and pH's. The solution EPR spectra were simulated using "two-dimensional" analysis which can consider all the recorded isotropic spectra simultaneously by fitting the isotropic EPR parameters and the overall stability constants of the defined species. Frozen solution (anisotropic) spectra were simulated individually which resulted the anisotropic EPR parameters of the species and their relative concentrations at each pH values. The isotropic and anisotropic EPR parameters calculated for the various species are found in Table 2. Best fit was obtained by taking into account complexes $[CuB]^{2+}$, $[CuBH_{-1}]^{+}$, an EPR inactive dimeric species $[Cu_2B_2H_{-2}]^{2+}$, $[CuBH_{-2}]^{2+}$, the bis complexes $[CuB_2]^{2+}$ and $[CuB_2H_{-1}]^{+}$, and the tris complex $[CuB_3]^{2+}$. (Notably, the complexes bearing H_{-1} component are mixed hydroxide species: $[CuBH_{-1}]^{+}$ = $[CuB(OH)]^{+}$), $[Cu_2B_2H_{-2}]^{2+}$ = $[Cu_2B_2(OH)_2]^{2+}$, $[CuBH_{-2}]^{2+}$ = $[CuB(OH)_2]^{2+}$, $[CuB_2H_{-1}]^{+}$ = $[CuB_2(OH)]^{+}$.) The obtained stability constants are similar to those obtained by the pH-potentiometric titrations and are comparable to those of Fábián et al. [43]. published previously (Table 1), the observed differences are due to the different media. The concentration distribution of copper(II) in the copper(II) – bpy system at various metal-to-ligand ratios are shown in Fig. S6. The experimental and the simulated solution EPR spectra are shown in Fig. S7. Detailed information about the geometry of the complexes can be gained by the evaluation of the frozen solution EPR spectra (Fig. S8). One by one simulation of the frozen solution (77 K) spectra yielded the component ratios at each pH which was depicted together with the distribution curves in Fig. S6.

Comparison of the obtained component ratios with the distribution curves calculated at room temperature can help in the assignment of the anisotropic spectrum components. The component spectra obtained from the simulation of solution and frozen solution EPR spectra are collected in Fig. 5. The spectra of complex $[CuB]^{2+}$ shows a moderate ligand field owing to the (N,N) coordination mode, however the linewidth of the spectra both at room temperature and at frozen solution does not allow the detection of the nitrogen splitting. Deprotonation of an equatorially coordinated water molecule increase the ligand field ($g_{\parallel}$ decreases while $A_{\parallel}$ increases) and decreases the linewidth in complex $[CuBH_{-1}]^{+}$, therefore the superhyperfine structure can be recognised in these spectra (Fig. 5). The nitrogen superhyperfine coupling has rhombic symmetry and the biggest value can be measured in the direction of the N—Cu bond, however in the other two directions the coupling has smaller values, so that two nitrogen couplings have been taking into account describing the (N,N) coordination, one with higher value at x and another at y direction (referring to the g-tensor). Dimerisation of complex $[CuBH_{-1}]^{+}$ through an OH^{-} bridge resulted in the EPR inactive dimer $[Cu_2B_2H_{-2}]^{2+}$ where the S = 0 overall spin is due

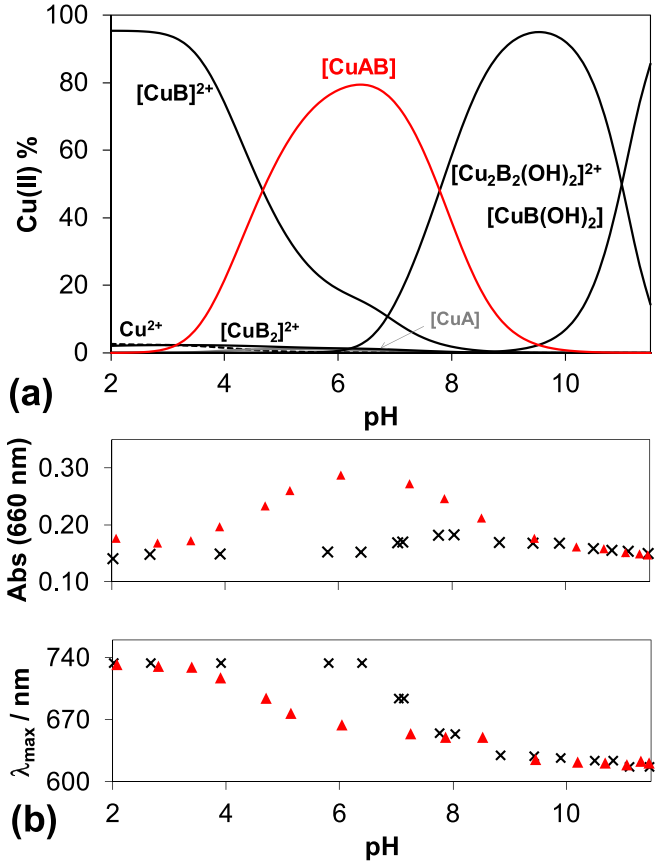

Fig. 4. Concentration of distribution curves of Cu(II) - phthalate (A^{2-}) - 2,2′-bpy (B) (1:1:1) ternary system on the basis of the determined stability constants (a) and absorbance at 660 nm and λ_{max} values for the Cu(II) - A^{2-} - B (1:1:1) ternary system (▲) and Cu(II) - B (1:1) binary system (×) for comparison (b). {30% (v/v) DMSO/H_2O; t = 25 °C, I = 0.10 M (KCl); $c_{Cu(II)}$ = 2 mM; l = 2 cm}.

to the antiferromagnetic coupling between the two copper centres. At very high pH another water deprotonation process occurs and complex [$CuBH_{-2}$] could be detected for which the most prominent spectral changes were found, namely higher A_z and A_o values were determined compared to those of [$CuBH_{-1}$]$^+$. At two-fold ligand excess the complex [CuB_2]$^{2+}$ is predominant between pH 3–10. The obtained inverse ($g_\perp > g_\parallel > 2.00$) EPR spectrum reflects a d_{z^2} ground state instead of the usual $d_{x^2-y^2}$ in this complex. The square planar coordination of the two bipyridine is hindered because of the close C_α-H protons therefore the trigonal bipyramidal structure with the coordination of an extra water or chloride ion is suggested based on the inverse spectrum [45]. Numerous measurements were made on the EPR spectra of [CuB_2]$^{2+}$ and to clarify

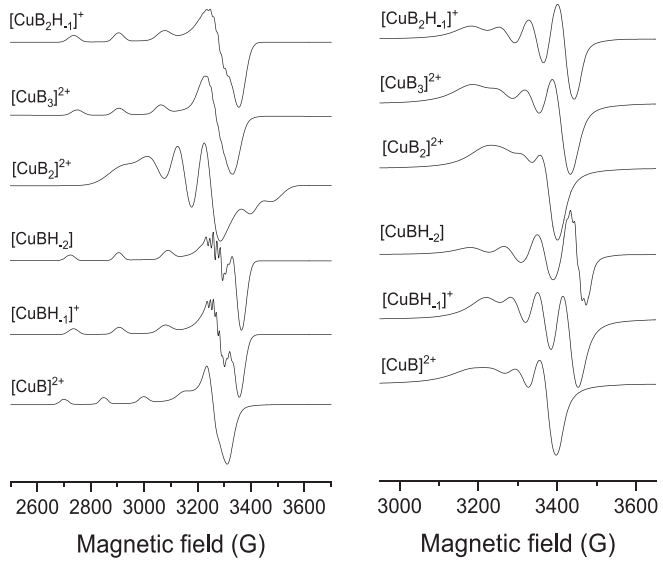

Fig. 5. Calculated anisotropic (left) and isotropic (right) EPR spectra of the components in copper(II)-bpy system.

Table 2
Isotropic and anisotropic EPR parameters of the components obtained in the copper(II) – phtalic acid (A) and copper(II) – bpy (B) binary and copper(II) – bpy (B) – phtalic acid (A) ternary systems[a].

	Isotropic EPR parameters[b]			*Anisotropic EPR parameters*[c]								*Calculated*[d]
	g_o	A_o^{Cu}	A_o^N	$g_\perp$ or g_x, g_y	$g_\parallel$ or g_z	$A_\perp^{Cu}$ or A_x^{Cu} A_y^{Cu}	$A_\parallel^{Cu}$ or A_z^{Cu}	A_x^{N1} A_x^{N2}	A_y^{N1} A_y^{N2}	A_z^{N1} A_z^{N2}	n° (N)	$g_{o,calc}$
[Cu(aqua)]	2.195	34.9		2.079	2.412	11	128					
[CuA]				2.063, 2.072	2.356	15, 12	152					2.164
[CuA_2]$^{2-}$				2.054, 2.072	2.348	18, 18	154					2.158
[CuB]$^{2+}$	2.1422 (1)	54.2 (1)	11.9	2.061	2.302	11	161					2.142
[$CuBH_{-1}$]$^+$	2.138(1)	55(2)	11(1)	2.049, 2.057	2.254	25, 15	177	10 13	12 10	9 11	1 1	2.120
[$CuBH_{-2}$]	2.1166 (1)	77.5 (1)	11.3 (2)	2.046, 2.054	2.251	27, 20	188	12 8	13 12	11 8	1 1	2.117
[CuB_2]$^{2+}$	2.1293 (2)	43.7 (1)		2.178	2.005	95	72					2.120
[CuB_2H_{-1}]$^+$	2.1238 (5)	65.0 (6)		2.052, 2.059	2.258	30, 11	174	11 11	14 8	13 8	2 1	2.123
[CuB_3]$^{2+}$	2.129(3)	64(3)		2.052, 2.065	2.263	18, 4	162	13 11	9 13	13 9	2 2	2.127
[CuAB]	2.128(3)	60(1)	12.1 (3)	2.045, 2.064	2.277	16, 2	176	14 13	7 12	13 8	1 1	2.1284
[$CuAB_2$]	2.123(4)	53(1)	8.0(5)	2.071	2.249	18	157					2.1300

[a] Coupling values are listed in 10^{-4} cm^{-1} unit.
[b] The numbers in parentheses are standard uncertainties of the quoted values.
[c] The experimental errors were ± 0.001 for g values, ± 2 × 10^{-4} cm^{-1} for A_x and A_y and ± 1 × 10^{-4} cm^{-1} for A_z and a^N.
[d] Isotropic values calculated via the equation $g_o = (g_x + g_y + g_z)/3$.

the differences it was also revisited by Garribba et al. in different solvents [45]. It was concluded that the geometry can change from tetragonal geometry to square pyramid or trigonal bipyramid depending on the solvation effect of the solvents. Like our case, a trigonal bipyramidal structure were detected for complexes $[Cu(bpy)_2OSO_3].4H_2O$ and $[Cu(bpy)_2ONO_2]NO_3.H_2O$ dissolved in pure MeOH. This trigonal bipyramidal structure was also detected for many bis-bipyridine copper (II) complexes in solid phase (Scheme S6.) [45,49]. At high pH the coordinated water molecule deprotonates and owing to the greater electronegativity of the OH^- ion the geometry shifts from the trigonal bipyramidal versus a square pyramidal where the OH^- coordinates in the equatorial plane and one bipyridine nitrogen highlight the axial position. Accordingly, the spectrum recorded at pH = 12.44 at three-fold ligand excess was described by considering the splitting of three nitrogen atoms (Fig. S7c and Table 1). At higher ligand excess the tris complex $[CuB_3]^{2+}$ could be detected in small amount (20%) at room temperature, however, at frozen solution the predominant formation of this complex was observed. The spectrum of this species has a usual g-tensor ($g_\parallel > g_\perp > 2.00$) supporting the more favoured elongated octahedral geometry which was also observed in single crystals [42,44](see Scheme S6b). This more favorable geometry explains its predominant formation under frozen solution conditions. The species $[Cu_2B_4H_{-1}]^{3+}$ detected by Fábián et al. cannot be excluded in a potentially EPR inactive form, as a small decrease in the EPR intensity could be observed, but this also can be due to the many overlapped species at around pH ~ 10.

2.3.3. *Copper(II) – phthalic acid (A) – 2,2′-bipyridine (B) ternary system*

For the description of the EPR spectra measured in the copper(II) - phthalic acid - bpy ternary system the component curves obtained in the copper(II) - phthalic acid and copper(II) - bpy binary systems were used. The experimental and simulated curves of frozen solution EPR spectra recorded at different Cu(II) – phthalic acid – bpy ratios and pH's are collected in Fig. S9. The component ratios obtained from the simulation are shown in Fig. S10. In the 1:1:1 and 1:2:1 copper(II) - phthalic acid - bpy ratios at acidic pH the $[CuB]^{2+}$ complex is predominant, however, a new component appeared at pH > ~4 which can be assigned as [CuAB] (Fig. 6, Table 1). The well-resolved nitrogen splitting indicates two equatorially coordinated nitrogen atoms in the latter complex. The single crystal structure of this mixed-ligand complex was already measured and reported giving a cyclic dimer $[CuAB]_2$ (Scheme S7). Our results exclude the formation of such dimer both at room temperature and in frozen solution, since the very close copper-copper distance (3.444 Å) would result in a significant line broadening or the appearance of a doublet peak, which was not observed in our experiments. Thus, we suggest that monomeric [CuAB] complex forms in solution. At higher pH the phthalate is replaced by one or two OH^- ions and the formation of $[CuBH_{-1}]^+$ and $[CuBH_{-2}]$ was detected. At 1:1:2 copper(II) - phthalic acid - bpy ratios the distribution of the species significantly changed. In acidic conditions beside the complex [CuB] the bis complex $[CuB_2]$ appeared and with increasing pH another mixed ligand complex $[CuAB_2]$ could be assigned. Notably, based on the pH-potentiometric and UV–vis titrations we could not determine stability constant for this species. The EPR spectrum and the parameters shows high ligand field ($g_z = 2.2488$ the smallest value in the series) with a $d^{2.2}_{x^2-y^2}$ ground state in this complex (Table 2). However, the A_z value is relatively low reflecting rhombic distortion. The g_z/A_z ratio is an empirical factor of tetrahedral distortion and this value is expected to be in the 105–135 and 150–250 range respectively for square planar and tetrahedral distorted copper(II) complexes [46,50]. In our case this value is 147 showing that the equatorially coordinated donor atoms are not fully in plane. All together these values support a distorted square pyramidal or elongated octahedral structure similar to those of a phthalic acid – phen mixed-ligand complex or a bpy – 3-nitro-2-carboxybenzoate complexes found in solid state (Scheme S3) [19,51]. In these cases, one bpy or phen ligand coordinates equatorially, the other one equatorially and axially, and the fourth equatorial position is occupied by the carboxylate oxygen of the phthalate acid or 3-nitro-2-carboxybenzoate. However, the other oxygen atom of the carboxylate group is very close to the second axial position. At higher pH again the OH^- group replaces the phthalate in the coordination sphere, and the complex $[CuB_2H_{-1}]^+$ becomes predominant. Isotropic EPR parameters of the mixed ligand complexes were determined by the simulation of selected solution EPR spectra at their concentration maxima (Fig. S11, Table 2).

Taking all of the speciation studies together, at physiological pH there is compelling evidence for the formation of a stable ternary [Cu(ph)(bpy)] species. However, with decreasing the concentration of the complex to the biologically more relevant range its fraction is decreased as the ternary complex partly dissociates to the Cu(II) complexes of 2,2′-bipyridine ($[Cu(bpy)]^{2+}$, $[Cu_2(bpy)_2(OH)_2]^{2+}$) and the free phthalate (Fig. S12). It is also noteworthy that based on the equilibrium constants it can be also assumed that the fraction of the free metal ion is negligible even at 1 μM concentration of the complex **3**.

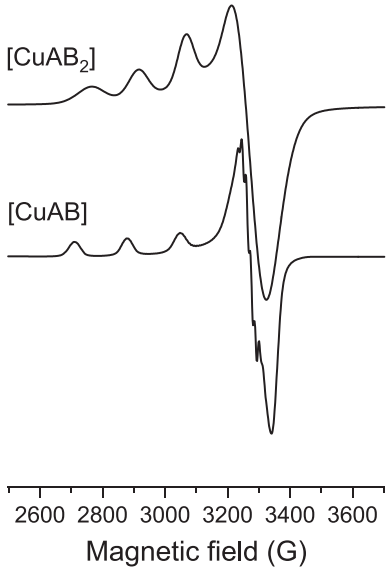

Fig. 6. Calculated anisotropic EPR spectra of the mixed-ligand complexes obtained in copper(II)-phthalic acid-bpy system.

2.4. *Biomimetic activity of complexes **1**–**3** in yeast cell model*

The SOD and CAT activities of complexes **1–3** were previously measured by the cell-free nitroblue tetrazolium (NBT) assays and by the ability of the complexes to disproportionate hydrogen peroxide respectively [24,39]. All three complexes had comparable SOD activity relative to the copper aspirinate control. In the absence of added imidazole, none of the complexes appears to show CAT activity, however in the presence of added base the complexes appeared to show moderate CAT activity, albeit less than that of the positive control, [Mn(II)(phthatale)(phen)(H_2O)]•H_2O. A previous study evaluated the antioxidant activity of Schiff base copper(II) complexes using a *Saccharomyces cerevisiae* model system as *S. cerevisiae* is a facultative anaerobe [36] and is a good eukaryotic model for determining the in vivo SOD and CAT-like activity of metal-based complexes [52,53]. Using this cell platform, the Schiff base complexes were shown to have the ability to act as SOD mimetics, but not CAT mimetics, despite all complexes showing dual ability measured using the same cell free assays mentioned above.

In this study, wild type yeast cells were grown in glucose rich media to mid-log phase of growth, when the endogenous antioxidant system (e.g. Mn- SOD and CAT activities) are down regulated [52,53]. Therefore, any SOD or CAT activity observed will be, as far as possible, the result of the antioxidant capability exhibited solely by the complex. Cytotoxicity of complexes **1–3** towards *S. cerevisiae* BY4741 wild type and *sod1Δ* and

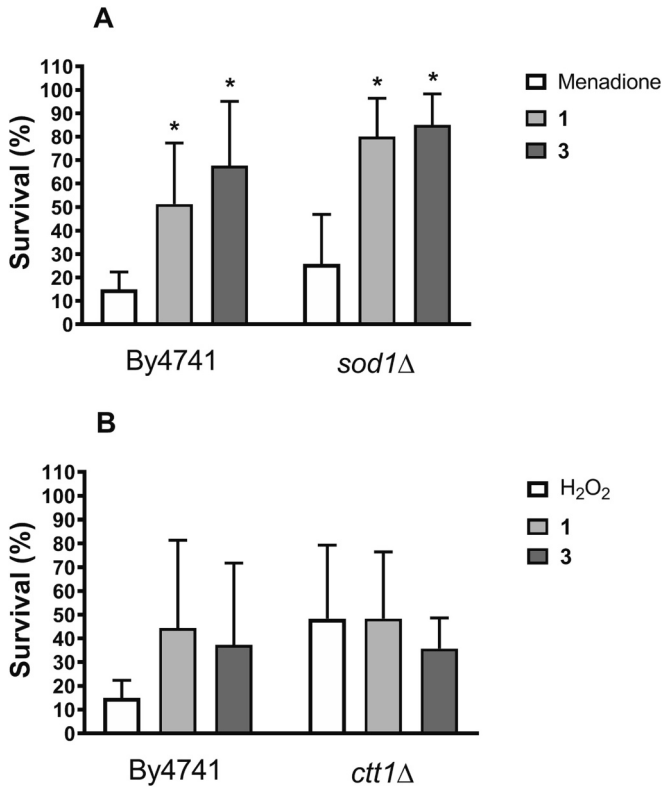

Fig. 7. (A) The effect of 2-h pre-incubation with 100 μM of complexes **1–3** on the survival rates of wild type *S. cerevisiae* cells exposed to 30 mM menadione. (B) The effect of 2-h pre-incubation with 100 μM of complexes **1–3** on the survival rates of wild type *S. cerevisiae* cells exposed to 2 mM H_2O_2. All results represent the mean ± SEM of cells plated in triplicate from 3 experiments.

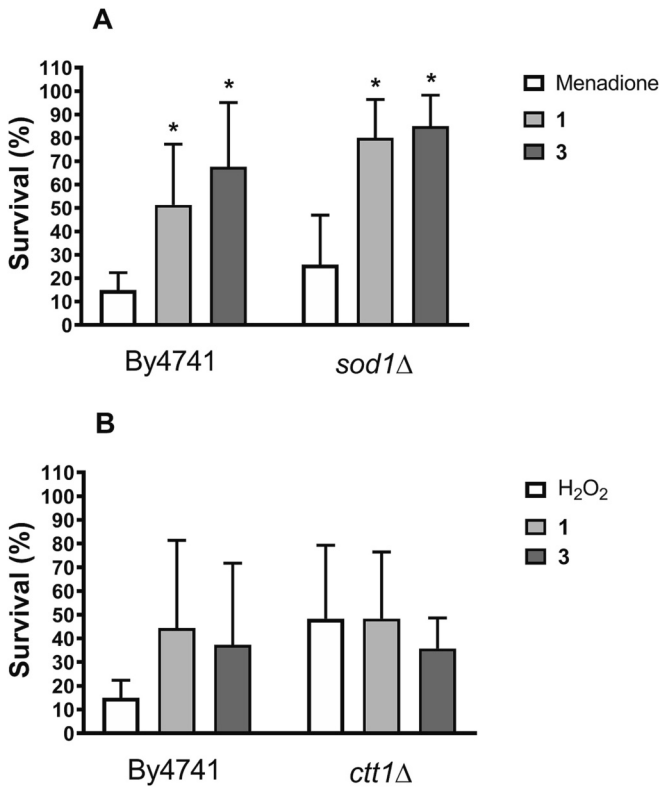

Fig. 8. The effect of 2-h pre-incubation with 100 μM of complexes **1** and **3** on the survival rates of the wild type and its isogenic *ctt1Δ* and *sod1Δ S. cerevisiae* mutants exposed to (A) menadione (1.2 mM/1 h) and (B) H_2O_2 (30 mM or 10 mM/1 h for wild type or *ctt1Δ*, respectively). The results represent the mean ± SEM of cells plated in triplicate from 3 experiments.

ctt1Δ mutant cells was assessed by treating each cell type with compounds at a concentration of 100 μM to observe any growth inhibition. No growth inhibition was observed indicating that the cells tolerated this concentration of copper(II) complexes, (Figs. S13 and S14). Cells were treated with sub-lethal concentrations of menadione or hydrogen peroxide to induce an oxidative response as positive controls. Test conditions involved cells which were pre-treated with compounds and subsequently treated with stressor to evaluate any potential protective effects of the metal complexes. The viable cell count recorded for the negative control, represented 100% survival and the positive controls and complex treated cells were calculated as a percentage of this.

Complex **1**, Fig. 7, showed statistically significant protection to the wild type cells subjected to $O_2^{\bullet-}$ and H_2O_2 stresses, with 81% and 47% of cells surviving when pre-treated with **1**, respectively. In this scenario, we observed a 3.0-fold increase ($P = 0.0339$) in survival under $O_2^{\bullet-}$ stress and a 2.5-fold increase under H_2O_2 stress. Complexes **2** and **3** also protected *S. cerevisiae* model (Fig. 7) against $O_2^{\bullet-}$ stress albeit no positive effect was observed under H_2O_2 stresses despite showing excellent biomimetic activity in cell-free assays. Complexes **1** and **3** was further studied to see if it could demonstrate SOD and CAT activity in the *sod1Δ* and *ctt1Δ* mutant cells. As the mutants are more sensitive to oxidative stress due to diminished defences, a lower concentration of stressor was required to treat the mutant cells compared to the wild type cells. Slower growth rates are observed in *sod1Δ* mutants under aerobic conditions, therefore a glucose-rich media was used to create fermentative conditions for the determination of SOD mimetic activity. A significant protective effect was observed with the pre-treatment of cells with complexes **1** or **3** in the *sod1* mutant cells (Fig. 8). CAT gene expression and activity is mostly repressed in yeast cells growing under fermentative conditions, and due to this characteristic, a non-repressor carbon source (glycerol) was used to induce CAT expression in growing yeast cells. Not surprisingly complex **1** and **3** protected both the wild type and *sod1* mutant cells exposed to $O_2^{\bullet-}$ stress, however, they did not demonstrate a protective effect in the CAT mutant studies. Thus, the biomimetic activity of the complexes identified in the cell free studies was partially replicated in the yeast model, since only the SOD mimetic activity was detected for all compounds.

*2.5. ROS generation of carboxylate-derived complexes **1–3** and their corresponding ligands in MCF-7 cells using ROS probe 2′,7′-dichlorodihydrofluorescein diacetate*

The ability of all three complexes to generate ROS in MCF-7 cells was assessed. Complex **1**, only showed statistically significant generation of ROS after 180 min at the highest concentration of 100 μM (Fig. 9a). Treatment with complex **2** gave an immediate concentration dependent, 2- to 29-fold increase at time zero (Fig. 9b). Complex **3** gave a 12-fold increase in ROS induction after 60 min at 100 μM concentrations, ($P = 0.0051$). After 120 and 180 min of incubation, an eight and six-fold increase in ROS induction at these respective time points was observed (Fig. 9c).

Copper acetate monohydrate, ligands bpy, phthalate, 3,5-diisopropylsalicylate (dips) and phen were also tested for their ability to generate ROS in MCF-7 cells (Fig. S15a-e). None of the ligands showed any ability to generate ROS. In contrast, the copper salt did show statistically significant ROS induction, after 180 min of incubation at 50 μM, but not at 100 μM after the same time period.

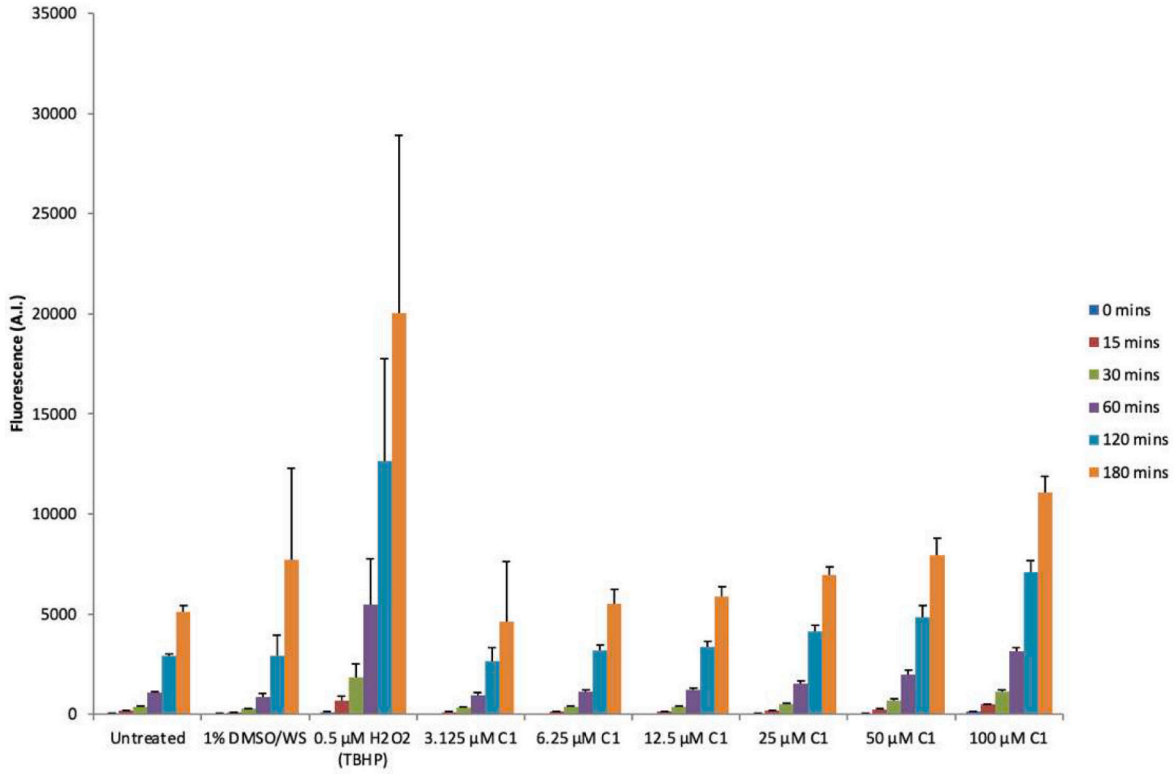

(a)

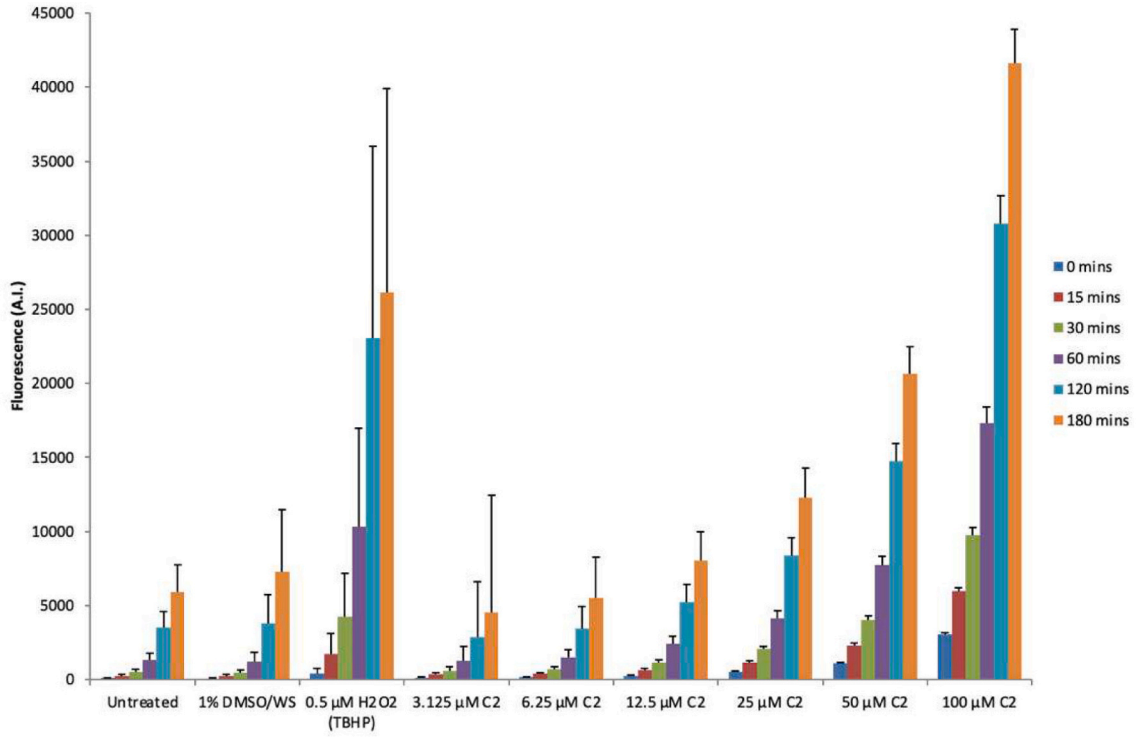

(b)

Fig. 9. Time-course generation of endogenous ROS within MCF-7 cells after exposure to increasing concentrations (3.125 µM – 100 µM) of (a) complex **1**, (b) complex **2** and (c) complex **3** over a time course of 0–180 min. Errors bars representative of SEM from 3 experiments.

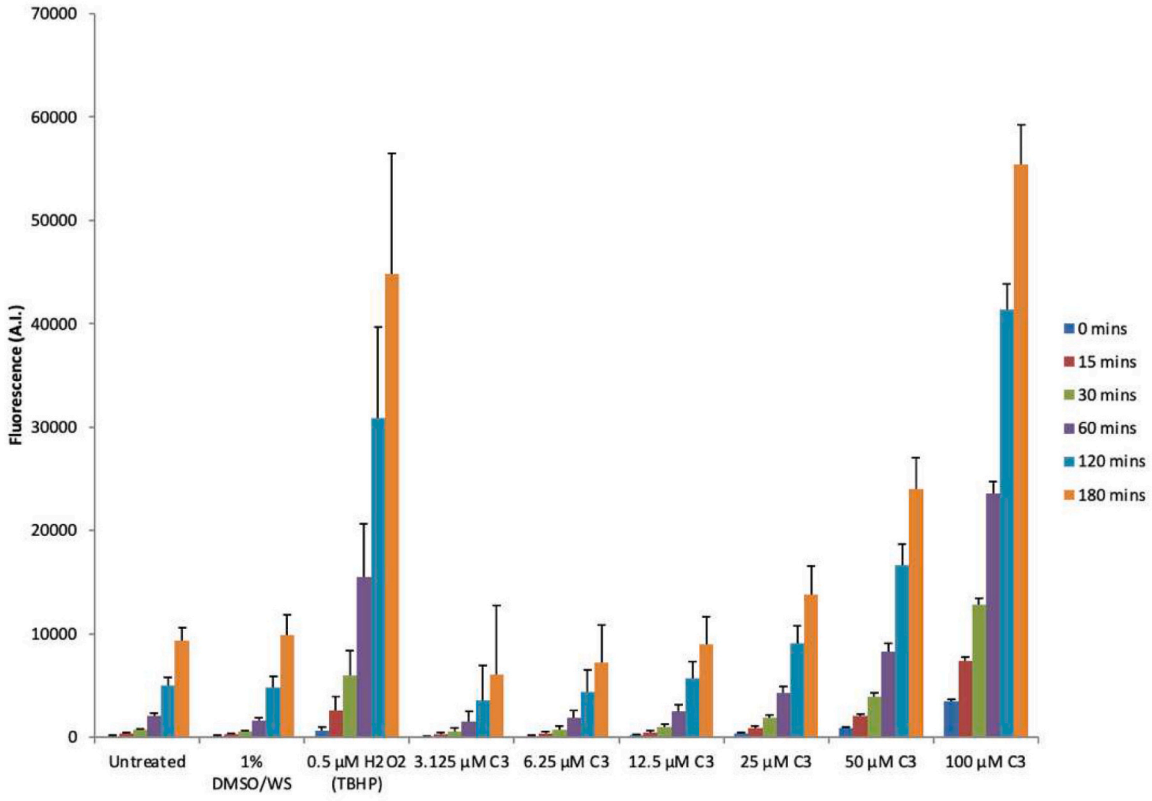

(c)

Fig. 9. (*continued*).

Table 3
IC_{50} values (μM) calculated from complex and drug treated MCF-7 cells in normoxic, hypoxic and anoxic conditions and for complex treated HaCaT cells in normoxic and hypoxic conditions after 24 h determined using MTT assay.

	MCF-7			HaCaT*	
	Normoxic 20% O_2 (μM)	Hypoxic 1% O_2 (μM)	Anoxic 0.1% O_2 (μM)	Normoxic 20% O_2 (μM)	Hypoxic 1% O_2 (μM)
Complex/ Drug	Ic_{50} value [μM]	Ic_{50} value [μM]	Ic_{50} value [μM]	Ic_{50} value [μM]	Ic_{50} value [μM]
Doxorubicin	71.6 ± 1.5	41.2 ± 4.7	> 100		
Cisplatin	96.2 ± 2.3	97.4 ± 0.05	> 100		
Mitoxantrone	15.0 ± 8.7	14.2 ± 3.0(2)	54 ± 9.3		
Complex 1	28.3 ± 10.1	9.2 ± 0.04	40.2 ± 7.9	34.6 ± 16	14.1 ± 9
Complex 2	13.3 ± 1.1	9.5 ± 4		65.4 ± 6	87.3 ± 14
Complex 3	62.8 ± 9.1	27.6 ± 11.6	67.5 ± 4.4	113.4 ± 28	324.0 ± 25

± Standard error of the mean, 3 independent experiments unless otherwise stated in parenthesis.
Standard error of the mean, 3 replicate experiments.

*2.6. Cytotoxicity of clinical drugs and complexes **1**–**3** against MCF-7 cells in normoxic, hypoxic and anoxic conditions and cytotoxicity of complexes **1**–**3** against HaCaT cells in normoxic and hypoxic conditions assessed using MTT assay*

The cytotoxicity of the complexes **1–3** was assessed in MCF-7 cells via the MTT viability assay in normoxic, and hypoxic conditions and the results presented in Table 3. Cells were grown in the relevant levels of oxygenation for 24 h across a concentration range of 0–500 μM. The complexes were also screened against the immortalised keratinocyte HaCaT cells under normoxic and hypoxic conditions via the same assay. In normoxic conditions the cytotoxicity of complex **1** in the HaCaT cell line was similar to its cytotoxicity in MCF-7 cells, IC_{50} values of 34.6 ± 16 μM and 28.3 ± 10.1 μM respectively but cytotoxicity was reduced in the HaCaT cell line for complex **2** relative to that in MCF-7 cells, IC_{50} values of 65.4 ± 6 μM and 13.3 ± 1.1 μM respectively, and likewise for complex **3**, IC_{50} values of 113.4 ± 28 μM in HaCaT cells and 62.8 ± 9.1 μM in MCF-7 cells.

Complex **1** was found to be more cytotoxic under hypoxic conditions to both the immortalised keratinocyte HaCaT cell line and MCF-7 cells, with IC_{50} values of 14.1 ± 9 μM in HaCaT cells and 9.2 ± 0.0 in MCF-7 cells respectively whereas the cytotoxicity of complex **2** towards HaCaT cells was significantly reduced relative to its cytotoxicity against MCF-7 cells, IC_{50} values of 87.3 ± 14 μM and 9.5 ± 4 μM respectively. The cytotoxicity of complex **3** in HaCaT cells under hypoxic conditions was greatly reduced with IC_{50} values of 324.0 ± 25 μM compared to its toxicity in MCF-7 cells under hypoxic conditions, with a comparative IC_{50} value of 27.6 ± 11.6 μM. The significant increase in cytotoxicity under hypoxic conditions of complexes **1** and **3** in MCF-7 cells, coupled with their contrasting behaviour in HaCaT cells, prompted the further study of the behaviour of the complexes, under anoxic conditions and the results are shown in Fig. 10 and summarised in Table 3.

Complex **1** shows IC_{50} values obtained were 28.3 ± 10.1, 9.2 ± 0.04 and 40.2 ± 7.9 μM in normoxic, hypoxic and anoxic conditions respectively, showing reduced effectiveness in anoxic conditions. Differences between treatments in normoxic and hypoxic, and hypoxic and anoxic conditions were found to be significant, ($P < 0.0001$), whereas there was no significance found between normoxic and anoxic

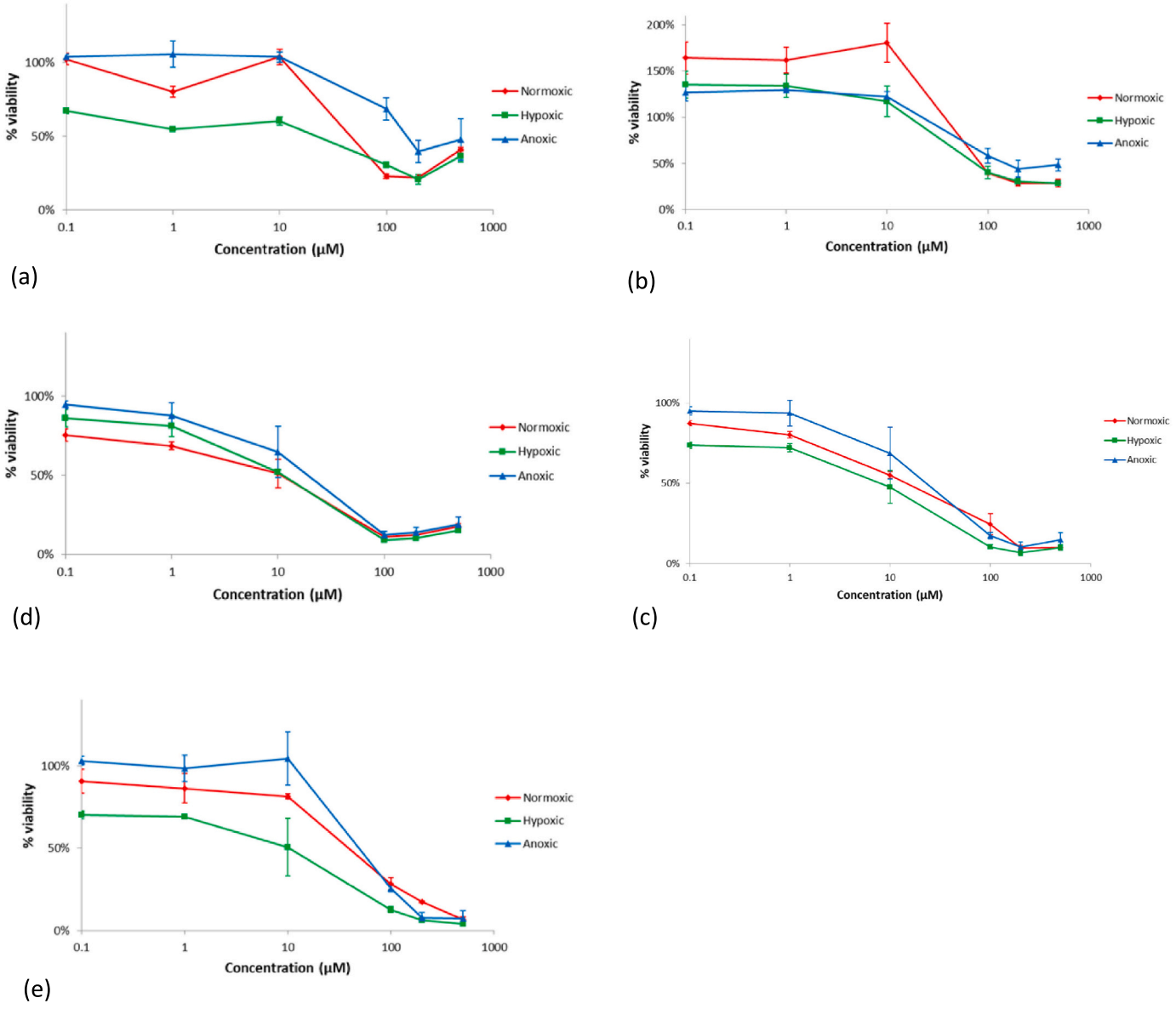

Fig. 10. The effect of 24 h pre-incubation in normoxic, hypoxic and anoxic environments on the cytotoxicity of (a) Doxorubicin, (b) Cisplatin, (c) Mitoxantrone, (d) complex **1** and (e) complex **3** against MCF-7 cancer cells after 24 h exposure. Error bars represent SEM from three independent experiments.

conditions. The same trend in results was also noted for complex **3.** Treatment of MCF-7 cells with complex **3**, resulted in substantial reduction in cell viability in hypoxic conditions even at the lowest concentration tested, suggesting that hypoxia enhances anticancer activity. Drug efficacy was statistically different between normoxic and hypoxic conditions ($P = 0.0001$) and between hypoxic and anoxic conditions ($P < 0.0001$), but no significant difference in effect was observed in normoxic conditions, relative to anoxic conditions again for complex **3.**

In addition to the studies on the three copper complexes under investigation the cytotoxicity of clinical drugs Doxorubicin, Cisplatin and Mitoxantrone, in all three oxygen conditions against MCF-7 cells were assessed via the MTT viability assay and the results also presented in Fig. 10 and summarised in Table 3. The sensitivity of MCF-7 cells towards Doxorubicin was statistically different between all oxygen levels, (all $P < 0.0001$) with Doxorubicin appearing to be the most effective as an anticancer agent when cells were grown in hypoxic conditions, and least effective in anoxic conditions as shown in Fig. 11a. The efficacy trend of Doxorubicin in MCF-7 cells was hypoxic>normoxic>anoxic, with IC_{50} values of 41.2, 71.6 and > 100 μM respectively. In a similar study carried out by Strese et al., MCF-7 cells were incubated at the longer incubation time of 72 h and the effectiveness of Doxorubicin against MCF-7 cells in the varying oxygen conditions mirrored that shown here i.e. hypoxic>normoxic>anoxic [34][34].

The trend found from previous studies by Strese et al. for the efficacy of Cisplatin against MCF-7 cells was anoxic>hypoxic>normoxic but that trend was not replicated here, Fig. 10b. Treatment of MCF-7 cells with known breast cancer drug Mitoxantrone followed similar trends in all conditions at higher concentrations, as seen in Fig. 10c. Treatment with Mitoxantrone was significantly more effective in normoxic conditions compared to anoxic conditions, ($P = 0.0378$), with hypoxic conditions having no effect on drug efficacy, relative to normoxic or anoxic conditions.

The statistical difference observed in the sensitivity of MCF-7 cells exhibited towards many of the drug and complex treatments in normoxic, hypoxic and anoxic conditions are shown together in Table S3. Overall in these studies, Cisplatin appeared to have the poorest

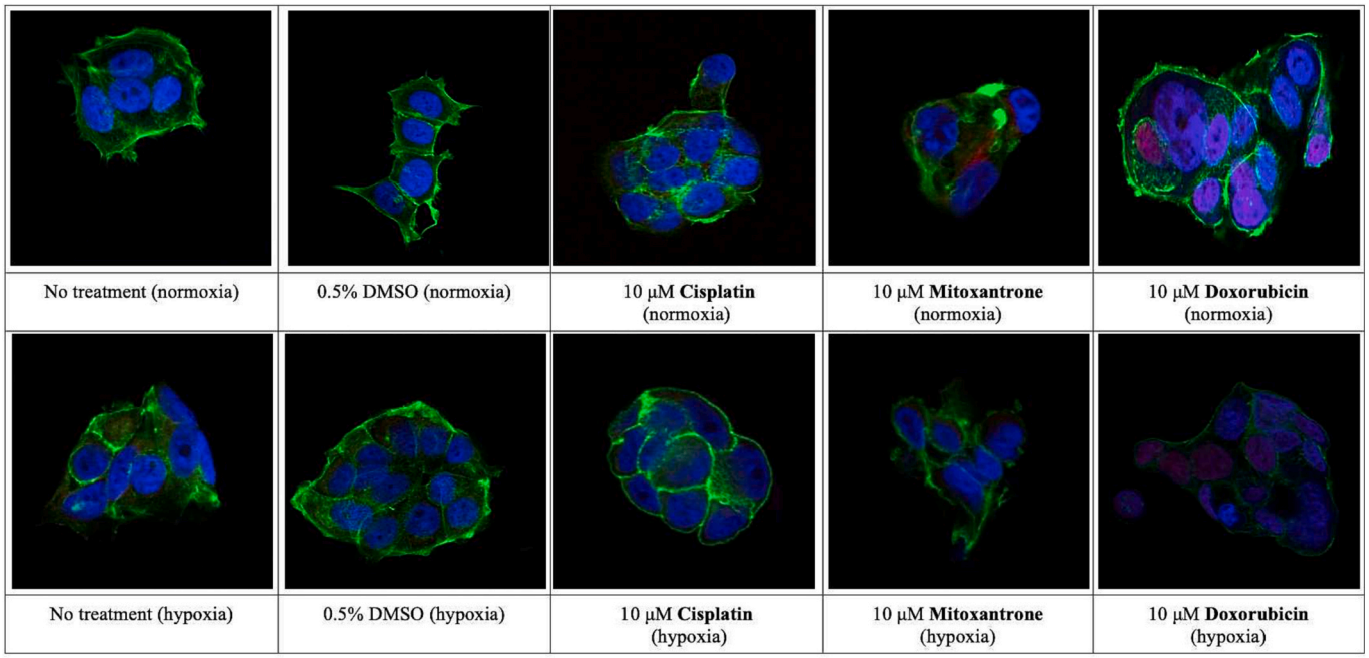

Fig. 11. 60× confocal images of MCF-7 cells treated with 0.5% DMSO control, 10 μM **Cisplatin**, 10 μM **Mitoxantrone** and 10 μM **Doxorubicin** under normoxic and hypoxic conditions, stained with Alexa Fluor 488 Phalloidin (green), DAPI (blue) and MitoTracker Red CMXRos (red). (For interpretation of the references to colour in this figure legend, the reader is referred to the web version of this article.)

anticancer activity out of the established drugs tested here, against MCF-7 cells in all conditions as shown in Table 3. It also appeared to lose efficacy with decreasing oxygen concentration, which fits in with the emerging Cisplatin-resistance exhibited by tumour cells. The most effective drug against MCF-7 cells was Mitoxantrone, an established clinical chemotherapeutic treatment for breast cancer but the efficacy of Mitoxantrone also tailed off in an anoxic environment. The anticancer effects of complexes **1** and **3** against MCF-7 cells increased in hypoxic conditions relative to normoxic, and then decrease when subjected to anoxic oxygen concentrations. This is an interesting result, as an anoxic environment is 0.1% oxygen, while hypoxia is 1% oxygen, therefore an increase of 0.9% in O_2 concentration had a significant improvement on drug efficacy against MCF-7 cells. This may raise issues in treatment of tumours, as due to the irregular architecture of anoxic and hypoxic regions, the efficacy of the drug would vary within a small vicinity. Complex **3** was significantly less toxic in HaCaT cells in hypoxic conditions, whereas complex **1** increased its cytotoxicity (Table 3), indicating possible different mechanism of action for the two complexes.

Given that it is well established that tumour cells display enhanced anaerobic glycolysis and altered metabolic pathways under hypoxia

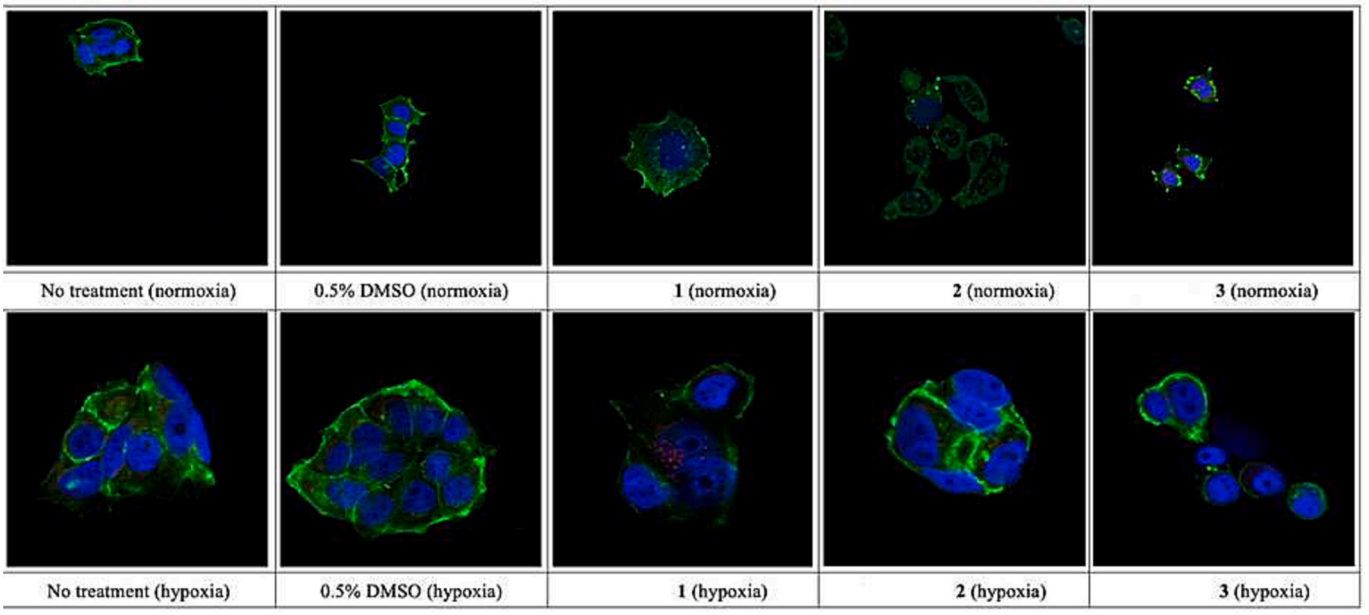

Fig. 12. x60 confocal images of MCF-7 cells treated with: Confocal images of MCF-7 cells grown and treated with IC_{20} concentrations of complexes **1–3 and** 0.5% DMSO control under normoxic and hypoxic conditions: stained with Alexa Fluor 488 Phalloidin (green), DAPI (blue) and MitoTracker Red CMXRos (red). * = x40 magnification. (For interpretation of the references to colour in this figure legend, the reader is referred to the web version of this article.)

[54], alternative targets for metal complexes may be available for cells in hypoxia and that may differ on the type of cell investigation. In addition, the likely switch to anaerobic metabolism in hypoxic and anoxic conditions means that reduction to copper(I) with a consequent change in coordination environment may target an alternative pathway or indeed switch on an increased cytotoxic response in reduced oxygen environments. A recent paper highlights a series of Cu(II) complexes with tridentate pyridine aminophenolate-based ligands which are preferential activated in the reduction window provided by hypoxic tissues [55]. In an effort to understand the basis of our results, and whether cell death was via different pathways under differing oxygen conditions, confocal analysis of MCF-7 cells treated with the three complexes and the clinically used drugs, grown under normoxic and hypoxic conditions, were undertaken.

*2.7. Confocal analysis of known anti-cancer drugs and complexes **1**–**3** in normoxia and hypoxia*

Morphological changes induced in the MCF-7 cell line following treatment with the clinical drugs and with the IC_{20} values of copper(II) complexes in normoxia and hypoxia were visualised using confocal microscopy and fluorescent staining. Three fluorescent dyes were employed; DAPI, Alexa Fluor 488 Phalloidin and MitoTracker red CMXRos to stain the nuclei, F-actin filaments, and mitochondria respectively. MCF-7 cells grown in optimal conditions, Fig. 12, displayed clusters of cells with rounded morphology, uniform nuclei (blue) and intact actin filaments visually stained green, all of which are characteristic of cellular health. Similar characteristics were demonstrated in the vehicle control, 0.5% (*v*/v) DMSO in normoxia. However, following hypoxic incubation, MCF-7 cells appeared slightly stressed through the appearance of actin aggregates in both controls, Fig. 11, as expected given that hypoxia is thought to induce apoptosis [56,57].

MCF-7 cells treated with Cisplatin demonstrated signs of intact uniform nuclei similar to the controls but demonstrated signs of apoptotic stress with contracted patches of brightly stained actin filaments. Under hypoxia, MCF-7 cells treated with Cisplatin, enlarged nuclei and actin condensation were visible [58,59]. Apoptotic characteristics such as lunate nuclei, diffuse staining of nuclei [60], depolarisation of mitochondria and some bright patches of actin filaments were demonstrated by MCF-7 cells treated with Mitoxantrone. Under hypoxia, MCF-7 cells treated with Mitoxantrone had poorly stained actin filaments relative to the controls and non-uniform nuclei. Similarly, mitochondria were devoid of staining which indicated reduced metabolic activity of these cells, suggesting the potential for apoptotic cell death. In normoxia and hypoxia, MCF-7 cells treated with Doxorubicin demonstrated signs of condensed bright actin filaments and non-uniform nuclei [59,60]. Additionally, signs of mitochondrial retrograde and dotted/punctate actin filaments indicated that cell death mediated through non-apoptotic cell death pathways occurred [61].

Signs of cellular stress including diffuse punctate staining of actin filaments and nuclei were evident following treatment of MCF-7 cells with **1** in normoxia, Fig. 12. Under hypoxia, nuclei and f-actin filaments were diffusely stained, non-uniform and lunate in shape. Treatment with **1** also induced signs of mitochondrial dysfunction. In normoxia, diffuse staining of nuclei and the formation of actin aggregates were evident in MCF-7 cells following treatment with **2**. Signs of apoptotic stress induced by **2** were exacerbated under hypoxia, in which non-uniform nuclei and condensed patches of actin filaments were evident. Signs of nuclear stress were not induced following treatment of MCF-7 cells with **3** in normoxia. However, the formation of apoptotic bodies and polarized mitochondria were indicative signs of apoptotic cell death. Treatment of MCF-7 cells with complex **3** under hypoxia induced the formation of non-uniform nuclei and condensed patches of actin filaments, which are considered classical signs of apoptosis. Thus, confocal studies confirmed that cell death induced by the copper(II) complexes appeared to be consistent with an apoptotic pathway in both normoxic and hypoxic conditions.

3. Conclusion

This work probed the relationship between biomimetic activity, ROS activity of selected copper(II) complexes and their anticancer activity under varying oxygen conditions. Solubility issues limited the solution speciation studies to complex **3** though the ternary nature of the [Cu(NN)(OO)] complex could be confirmed at physiological pH, although its partial dissociation takes place with decreasing concentration. Chemotherapeutics whose mechanism of action is based on generation of ROS and subsequent DNA or, mitochondrial damage have been of interest for many years and in this study the cytotoxicity of three complexes, [Cu(dips)(phen)](**1**), [Cu(ph)(phen)]·$2H_2O$(**2**) and **[**Cu(ph)(bpy)]·H_2O(**3**) (disp: 3,5-diisopropylsalicylate, phen: 1,10- phenanthroline, ph: phthalate, bpy: 2,2′-bipyridyl) was probed under varying oxygen conditions in MCF-7 cells and to a more limited extent in HaCaT cells. ROS generation for all three complexes in the MCF-7 breast cancer derived cell line was established using the DFCDA assay with complex **2** > complex **3** >> > complex **1** but that did not correlate with the cytotoxicity of the complexes under normoxic conditions, complex **2** > complex **1** > complex **3**. A recent paper focussed on the anticancer activity against HeLa cervical cancer cells of a series of mixed ligand Cu(II) complexes of the type [Cu(L)(diimine)](ClO_4), where the HL is 2-formylpyridine-N^4-phenylthiosemicarbazone and the diimine was either bpy, 4,4′-dimethyl-2,2′-bipyridine, phen, 5,6-dimethyl-1,10-phenanathroline or 3,4,7,8-tetramethyl-1,10-phenanthroline. Interestingly in their studies they noted that the complex with the 5,6-dimethyl-1,10-phenanathroline co-ligand, though most cytotoxic, was one of the least efficient ROS generators under normoxic conditions [62]. This complex however had increased ability to cleave DNA under hypoxic conditions but unfortunately, these studies did not include measurement of cytotoxicity under hypoxic conditions.

Studies on MCF-7 cells in normoxic, hypoxic and anoxic conditions identified that complexes **1** and **3** were considerably more cytotoxic under hypoxic conditions relative to the same complexes incubated in normoxic conditions whilst complex **2** held its original cytotoxicity. In comparison in the immortalised keratinocyte HaCat cells, the cytotoxicity of complexes **2** and **3**, was less under both normoxic and hypoxic conditions in fact reducing significantly for complex **3** under hypoxic conditions, but the cytotoxicity of complex **1** increased in that cell line. At the same time the cytotoxicity of three clinical anti-cancer drugs in varying oxygen conditions was also assessed. Unsurprisingly MCF-7 cells have been shown previously to be resistant to Cisplatin and oxygen conditions did not affect its cytotoxicity but Doxorubicin was more cytotoxic in hypoxia and the cytotoxicity of Mitoxantrone was unaffected. However, in very low oxygen conditions, perhaps because cells under those conditions switch to anaerobic respiration, only Mitoxantrone retained any activity against the cells. Whereas complexes **1** and **3** held their activity in anoxic conditions. Confocal microscopy studies that identified apoptotic features in MCF-7 cells treated with all three complexes and increased evidence for apoptosis when cells were incubated under hypoxic conditions.

The increased toxicity of complex **1** in hypoxic conditions for both MCF-7 and HaCaT cells**,** given the poor ROS generation by this complex, argues against ROS generation as a general mechanism to explain cytotoxicity of this type of copper(II) complex. Using a yeast cell platform, it was confirmed that complex **1** had the ability to act as an SOD mimetic, but its inability to generate ROS meant that its pro-oxidant potential as an SOD mimetic did not result in enhanced cytotoxic in this case. That fact correlated with complex **1**'s increased cytotoxicity in both cells line under hypoxic conditions indicating that this complex may not exert its cytotoxic effect through generation of ROS. A recent review of the role of metal complexes in anticancer therapy has highlighted metal complexes may well be implicated in a number of other redox processes including regulating or altering the activity of

oxidoreductases such as PHD2 (prolyl hydroxylase domain-containing protein) which can regulate angiogenesis in tumours, LDH (lactate dehydrogenase) related to glycolysis, and enzymes, such as catalases, SOD (superoxide dismutase), TRX (thioredoxin) or GSH (glutathione) all of which are involved in controlling oxidative stress [63].

Previous studies have shown the ability of copper(II) polypyridyl complexes to act as SOD mimetics, and convert metabolic superoxide to the pro-oxidant hydrogen peroxide and this ability coupled with the redox behaviour of this type of complex has long been proposed to enhance the anticancer activity of this type of complex. The phen complex **2** and bipy complex **3** did have SOD-mimetic activity and the ability to generate ROS but interestingly their cytotoxicity increased under hypoxic conditions for the cancer derived cell-line MCF-7 but was reduced in the immortalised keratinocyte HaCaT cell line, significantly so for complex **3**. Thus this study has shown that the cytotoxicity and the basis of that cytotoxicity is cell-line dependent and generalisations to ROS-based anticancer behaviour of these types of copper(II) complexes should not be made. The study did identify that these copper(II) complexes did hold their cytotoxicity in both hypoxic and anoxic conditions to a far greater extent than the clinically used anticancer drugs used to treat breast cancer. Future studies will focus on the exact role that copper complexes in cancer cells play when oxygen status within the cell is varied and correlate those studies which the species which exist at those concentrations. Hopefully these studeieswill identify cellular targets or pathways that can be targeted in hypoxic tissues by copper(II) based chemotherapeutics.

4. Experimental

4.1. General

Glacial acetic acid (Fisher Scientific), 18 MΩ·cm^3 (Elga tap), copper (II) chloride 3,5-diisopropylsalicylic acid, 1,10-phenanthroline, phthalic acid, copper(II) acetate monohydrate, 2,2′-bipyridine were purchased from Alfa Aesar. Potassium hydrogen phthalate, KCl, HCl, KOH and DMSO were purchased from Sigma-Aldrich in *puriss* quality. $CuCl_2$ stock solution was made by the dissolution of anhydrous $CuCl_2$ in water and its exact concentration was determined by complexometry through the EDTA titration. All solvents were of analytical grade and used without further purification. Doubly distilled Milli-Q water was used for sample preparation.

For the studies on wild type strain of *S. cerevisiae* cells, chemicals and solvents were purchased from Sigma Aldrich Brazil, Ltd., were of reagent grade and were used without further purification. Dehydrated media was purchased from Becton, Dickinson and Company, Brazil and were prepared in distilled water. Cultures were grown in a New Brunswick Scientific Innova®44 Incubator Shaker at 160 rpm 28 °C.

The majority of cell culture materials were supplied by Sigma Aldrich unless otherwise stated; Trypsin-EDTA solution, 10× (Sigma), fetal bovine serum (Sigma), penicillin-streptomycin 10,000 units penicillin and 10 mg streptomycin (Sigma,), L-glutamine 200 mM (Sigma), MEM non-essential amino acid solution, 10× (Sigma), sodium pyruvate solution 100 mM (Sigma), dimethyl sulfoxide suitable for cell culture (Sigma), Gibco MEM, no glutamine, no phenol red (Biosciences), Gibco PBS pH 7.4 (Biosciences), Trypan blue solution, 0.4% (Ampesco,), MTT {3-[4,5-dimethylthiazole-2-yl]-2,5-diphenyltetrazolium bromide} (Sigma), Formaldehyde ≥36% in H_2O (Sigma), Triton X-100 for molecular biology (Sigma), poly-L-lysine 0.01% (Sigma), Prolong gold (Thermofisher scientific), Alexfluor-488 Phalloidin (Thermofisher scientific), DAPI (4′,6-Diamino-2-phenylindole, dihydrochloride) (Thermofisher scientific), Mitotracker red CMX-ROS (Thermofisher), TBHP {Tertbutylhydroperoxide} (Merck), DCFDA {2′,7′-dichloodihydrofluorescein diacetate} (Thermofisher scientific), Propidium iodide (BD Biosciences, 556,419), FITC – Annexin V (BD Biosciences), Annexin V: binding buffer, 10× concentrate (BD Biosciences).

Infrared spectra were recorded as KBr discs in the region of 4000–400 cm^{-1} on an IR Prestige-21 Shimadzu infrared spectrometer. The elemental composition analyses (%CHN) were carried out in the Microanalytical Laboratory, Department of Chemistry, University College Dublin, Belfield, Dublin 4. Decomposition temperatures were recorded on a Stuart scientific SMP1 melting point apparatus and were taken up to a temperature of 390 °C. An Orion 710 A pH-meter equipped with a Metrohm combined electrode (type 6.0234.100) and a Metrohm 665 Dosimat burette were used for the titrations. A Hewlett Packard 8452 A diode array spectrophotometer was used to record the UV–vis spectra in the 200 to 950 nm window. The path length was 1 cm All EPR spectra were recorded with a BRUKER EleXsys E500 spectrometer (microwave frequency 9.81 GHz, microwave power 10 mW, modulation amplitude 5 G, modulation frequency 100 kHz). The isotropic EPR spectra were recorded at room temperature in a circulating system. For all hypoxic incubation a Whitely H35 Hypoxystation was humidified and set to 5% CO_2, 1% O_2 and 94% N_2, with continuous monitoring. The chamber was calibrated weekly within the range of 0.1% - 20% O_2, to maintain accurate oxygen conditions within this range.

Confocal imaging was carried out on a Leica SP DMi8 microscope equipped with a 100×/63× oil immersion objective and using HyD SMD detectors. Excitation was carried out using a pulsed White Light Laser, with a line at 488 nm for the Alexa Fluor 488 and a line at 572 nm for the Mitotracker Red. DAPI was excited with a Picoquant pulsed 405 nm laser. Images were acquired sequentially to reduce the possibility of signal bleed-through between the different dyes.

4.2. Speciation studies

4.2.1. Potentiometric titrations and calculations

The pH-potentiometric measurements for the determination of the proton dissociation constants of bpy and phthalic acid and the overall stability constants of the Cu(II) complexes were carried out at 25.0 ± 0.1 °C in DMSO:water 30:70 (*v*/v) as solvent and at an ionic strength of 0.10 M (KCl) used in order to keep the activity coefficients constant. The titrations were performed with carbonate-free KOH solution of known concentration (0.10 M). The concentrations of the base and the HCl were determined by pH-potentiometric titrations. An Orion 710 A pH-meter equipped with a Metrohm combined electrode (type 6.0234.100) and a Metrohm 665 Dosimat burette were used for the titrations. The volume resolution of the burette is 0.001 mL and its precision is 0.002 mL. The electrode system was calibrated to the pH = $-\log[H^+]$ scale in the DMSO/water solvent mixture by means of blank titrations (strong acid vs. strong base: HCl vs. KOH), similarly to the method suggested by Irving et al., [64] in pure aqueous solutions. The average water ionization constant pK_w was 14.53 ± 0.1, which corresponds well to the literature data [65]. The reproducibility of the titration points included in the calculations was within 0.01 pH. The pH-metric titrations were performed in the pH range 2.0–12.0. The initial volume of the samples was 10.0 mL. The ligand concentration was 2 mM and metal ion-to-ligand ratios of 1:1–1:4 were used for the binary complexes. In the case of the ternary system the Cu(II) concentration was kept constant (1 mM) and Cu(II):phthalate:bpy ratios were varied as 1:1:1; 1:2:1; 1:1:2 and 1:2:2. Samples were deoxygenated by bubbling purified argon through them for approximately 10 min prior to the measurements. Argon was also passed over the solutions during the titrations. The exact concentration of the ligand stock solutions together with the proton dissociation constants were determined by pH-potentiometric titrations with the use of the computer program HYPERQUAD [66]. The same program was also utilized to establish the stoichiometry of the complexes and to calculate the stability constants ($\log\beta(M_pL_qH_r)$). $\beta(M_pL_qH_r)$ is defined for the general equilibrium $pM + qL + rH \rightleftharpoons M_pL_qH_r$ as $\beta(M_pL_qH_r) = [M_pL_qH_r]/[M]^p[L]^q[H]^r$, where M denotes the metal ion and L the completely deprotonated ligand. The standard deviation of the $\log\beta$ values of species included into the model was always lower than 0.1. In all calculations exclusively titration data were used from experiments in which no precipitate was visible in the reaction mixture.

4.2.2. UV–vis spectrophotometric titrations

A Thermo Scientific Evolution 220 spectrophotometer was used to record the UV–vis spectra in the 200–1000 nm window. The path length was 2 cm. Stability constants of the Cu(II) complexes and the individual spectra of the species were calculated with the computer program PSEQUAD [67]. The spectrophotometric titrations were performed on samples containing Cu(II) ions at 2 mM concentration in the pH range from 2 to 12.0 at 25.0 ± 0.1 °C in DMSO:water 30:70 (*w*/w) at an ionic strength of 0.10 M (KCl). The concentration of the ligands was 2 or 4 mM. Measurements for 1:1 Cu(II)-to-bpy system were also carried out by preparing individual samples in which KCl was partially or completely replaced by HCl; pH values, varying in the range ca. 1.0–2.0 were calculated from the strong acid content.

4.2.3. EPR spectroscopic measurements and deconvolution of the spectra

X-band CW-EPR spectra were recorded with a BRUKER EleXsys E500 spectrometer (microwave frequency 9.81 GHz, microwave power 10 mW, modulation amplitude 5 G, modulation frequency 100 kHz). The isotropic EPR spectra were recorded during a titration using a circulating system. All titrations have been done at room temperature in 30% DMSO/water solution at $I = 0.10$ M (KCl). EPR spectra were recorded for copper(II)-bipyridine in equimolar solution of 2.0 mM concentration and in two fold and three fold ligand excess at 1.0 mM copper(II) concentration between pH 1.9 and 12.5. For copper(II)-phthalic acid equilibrium system two titrations have been performed in equimolar solution at 2.0 mM concentration and in three fold excess at 1.0 mM copper(II) concentration. To investigate the copper(II)-phthalic acid-bipyridine ternary system 1.0 mM copper(II) concentration was used and titrations at 1:1:1, 1:2:1 and 1:1:2 copper(II): phthalic acid: 2,2′-bipyridine molar ratios have been performed. KOH solution was added to the stock solution to adjust the pH which was measured with a Radiometer PHM240 pH/ion Meter equipped with a Metrohm 6.0234.100 glass electrode. A Heidolph Pumpdrive 5101 peristaltic pump was used to circulate the solution from the titration pot through a capillary tube into the cavity of the instrument. The titrations were carried out under nitrogen atmosphere. 0.1 mL of sample was taken out of the stock solution at various pH values and was measured individually in a dewar containing liquid nitrogen (at 77 K) under the same instrumental conditions as the room-temperature spectra described above.

Series of pH-dependent room-temperature CW-EPR spectra were simulated simultaneously by the „two-dimensional" method using the 2D_EPR program [68]. Each component curve was described by the isotropic EPR parameters g_o, A_o^{Cu} copper hyperfine and A_o^N nitrogen hyperfine couplings, and the relaxation parameters α, β, γ which define the line widths through the equation $\sigma_{MI} = \alpha + \beta M_I + \gamma M_I^2$, where M_I denotes the magnetic quantum number of copper nucleus. The concentrations of the complexes were varied by fitting their formation constants $\beta(M_pL_qH_r)$ defined by the general equilibrium described in the pH-potentiometric studies section. The anisotropic spectra, recorded at 77 K, were analyzed individually with the EPR program [65] which gives the anisotropic EPR parameters g_x, g_y, g_z (rhombic g-tensor), A_x^{Cu}, A_y^{Cu}, A_z^{Cu} (rhombic copper hyperfine tensor) and A_x^N, A_y^N, A_z^N (rhombic nitrogen superhyperfine tensor) and the orientation dependent line width parameters. All tensors were supposed as coaxial. Since a natural $CuCl_2$ was used for the measurements, the spectra were calculated as the sum of the spectra of ^{63}Cu and ^{65}Cu weighted by their natural abundances. The quality of fit was characterized by the noise-corrected regression parameter R_j. The details of the statistical analysis were published previously [69]. The copper and nitrogen coupling constants and the relaxation parameters were obtained in field units (Gauss = 10^{-4} T).

4.3. X-ray crystallography

Green crystals of complex **1**, suitable for X-ray diffraction, were obtained by diffusion of hexan into dichloromethane (DCM) solution of this compound. X-ray diffraction data were collected at room temperature at 20 °C using Mo-*K*α radiation on a Rigaku RAXIS-RAPID II diffractometer. Numerical absorption correction was carried out using the program CrystalClear [70], Sir2014 [71] and SHELXL [72] under WinGX [73] software were used for structure solution and refinement, respectively and the structures were solved by direct methods. The models were refined by full-matrix least squares on F^2. Refinement of non-hydrogen atoms was carried out with anisotropic temperature factors. Hydrogen atoms were placed into geometric positions, they were included in structure factor calculations, but they were not refined. The isotropic displacement parameters of the hydrogen atoms were approximated from the U(eq) value of the atom they were bonded to. The summary of data collection and refinement parameters are collected in Table S1. Selected bond lengths and angles of compounds were calculated by PLATON [74] software and the graphical representation and the edition of CIF files were done by Mercury [75] and enCifer [76] software, respectively. CCDC-2204359 (complex 1) contains the supplementary crystallographic data for this paper. These data can be obtained free of charge from The Cambridge Crystallo-graphic Data Centre via www.ccdc.cam.ac.uk/data_request/cif.

4.4. Biological studies

4.4.1. Antioxidant assays

Procedures for this assay have been published previously [77] and full details are given in Supplementary Information.

4.4.2. Cytotoxicity assay

MCF-7 Human Breast Cancer cells were sourced from the American Tissue Culture Collection (ATCC, USA). MCF-7 cells are an adherent cell line which were grown in Minimum Essential Medium Eagle with 1% (v/v) L-glutamine, 1% (v/v) penicillin-streptomycin solution containing 10000 units penicillin and streptomycin 10 mg/mL, 10% (v/v) Fetal Bovine Serum, 1% v/v sodium pyruvate 100 mM solution and 1% (v/v) MEM Non-Essential Amino Acid solution 100×.

These cells were grown in T75 cm^2 tissue culture flasks at 37 °C in a humidified atmosphere at 5% CO_2, unless grown under hypoxic condition in which the oxygen concentration was reduced to 1%, with all other factors remaining constant. Cells were fed as needed (every 2 days) between splitting and sub-cultured at ~80% confluency. Thiazolyl Blue Tetrazolium Bromide (MTT) cytotoxicity assay in MCF-7 cells was carried out according to a previously published procedure [36]. Three independent experiments were carried out and the IC_{50} values after 24 h of complex/ligands/drug treatment were determined relative to a negative control (cells not treated with complex).

The HaCaT cell line were sourced from the American Tissue Culture Collection (ATCC, USA) and is a non-cancerous normalized epithelial cell line cultured in minimum essential media supplemented with 1% sodium pyruvate solution, 1% non-essential amino acid solution, 1% L-glutamine and 10% FBS. These cells were grown in T75 cm^2 tissue culture flasks at 37 °C in a humidified atmosphere at 5% CO_2, unless grown under hypoxic condition in which the oxygen concentration was reduced to 1%, with all other factors remaining constant. Cells were fed as needed (every 2 days) between splitting and sub-cultured at ~80% confluency. Thiazolyl Blue Tetrazolium Bromide (MTT) cytotoxicity assay in MCF-7 cells was carried out according to a previously published procedure [36]. Three biological replicates were carried out and the IC_{50} values after 24 h of complex treatment and were determined relative to a negative control (cells not treated with complex).

4.4.3. ROS generation assay using 2′,7′-dichlorodihydrofluorescein diacetate (H_2DCFDA) fluorescent dye

The procedure used was published previously, and full details are given in supplementary information [36].

4.4.4. Confocal analysis

Prior to seeding MCF-7 cells, cover slips were coated with 1 mL of a 0.1% solution of poly-L-lysine for 2 h. Both cell lines were seeded at a density of 4×10^4 cells/mL in minimum essential medium (phenol red-free media), at a volume of 1 mL in a 35 mm culture dish containing 25 mm cover slips and incubated for 24 h prior to treatment. Following incubation, the cells were treated with the desired concentration of complex, cancer drug or control for 24 h prior to staining. The media was removed from the tissue culture dish and the coverslip was washed twice with 1 mL prewarmed sterile PBS. This solution was removed and 200 μL of Mitotracker red dye (150 nM) was added and incubated in darkness for 30 min at 37 °C. The coverslips were washed twice with 1 mL sterile PBS and subsequently fixed with 2 mL 3.7% formaldehyde for 10 min at room temperature in complete darkness. The washing procedure was then repeated followed by incubation with 1 mL 0.1% triton X-100 for 5 min in complete darkness at room temperature. The coverslips were then washed twice with 1 mL PBS and incubated with 200 μL of Alexa Fluor 488 Phalloidin (5 units/ml) for 30 min in complete darkness at room temperature. The coverslips were washed twice with 1 mL PBS and 200 μL of DAPI (300 nM) was added for 15 min in complete darkness at room temperature. Lastly, the coverslip was washed twice with 1 mLPBS and allowed air dry before mounting onto a slide.

CRediT authorship contribution statement

Hollie Jenkins: Formal analysis, Investigation, Methodology, Writing – original draft, Writing – review & editing, Data curation. **Louise MacLean:** Formal analysis, Investigation, Methodology, Writing – original draft, Writing – review & editing, Data curation. **Siobhán McClean:** Supervision, Writing – original draft, Writing – review & editing. **Gordon Cooke:** Supervision, Writing – review & editing. **Michael Devereux:** Funding acquisition, Writing – review & editing. **Orla Howe:** Supervision, Writing – review & editing. **Marcos D. Pereira:** Funding acquisition, Formal analysis, Writing – original draft, Writing – review & editing. **Nóra V. May:** Funding acquisition, Formal analysis, Supervision, Writing – original draft, Writing – review & editing. **Éva A. Enyedy:** Funding acquisition, Formal analysis, Supervision, Writing – original draft, Writing – review & editing. **Bernadette S. Creaven:** Funding acquisition, Conceptualization, Supervision, Writing – original draft, Writing – review & editing, Data curation, Project administration.

Declaration of Competing Interest

The authors declare the following financial interests/personal relationships which may be considered as potential competing interests.

Bernadette S. Creaven reports financial support was provided by Science Foundation Ireland and the Irish Research Council. Eva Enyedy reports financial support was provided by National Research Development and Innovation Office. Marcos D. Periera reports financial support was provided by Carlos Chagas Filho Foundation for Research Support of Rio de Janeiro State. Bernadette S. Creaven reports financial support was provided by Programme for Research in Third Level Institutions. The authors declare no other conflicts of interest.

Data availability

Data will be made available on request.

Acknowledgements

This work was funded by Science Foundation Ireland –Investigator Programme SFI/12/IP/1390, Irish Reseach Council Postgraduate Awards (EM 200701) and the Centre of Applied Science for Health, *TU Dublin - Tallaght Campus, Tallaght, D24 FKT9*. This work was also supported by the National Research, Development and Innovation Office (Hungary) through project TKP-2021-EGA-32 and by the "Lendület" Programme (ELKH, LP2019-6/2019) (EAE) and the OTKA project K124544. Additional support was proved under FAPERJ (Edital N.° 43/2013, Programa de Apoio ao Doutorado-Sanduíche Reverso), CNPq and CAPES fundings. Confocal imaging was carried out at the Nano Research Facility in Dublin City University which was funded under the Programme for Research in Third Level Institutions (PRTLI) Cycle 5 under the supervision of Dr. Úna Prendergast. The PRTLI is co-funded through the European Regional Development Fund (ERDF), part of the European Union Structural Funds Programme 2011–2015.

Appendix A. Supplementary data

Supplementary data to this article can be found online at https://doi.org/10.1016/j.jinorgbio.2023.112383.

References

[1] Organisation WH, Cancer: World Health Organisation, Available from: https://www.who.int/health-topics/cancer#tab=tab_1, 2023.
[2] Union E, Breast cancer Burden in EU-27, European Union, 2020.
[3] Chemotherapy for Breast Cancer: American Cancer Society, Available from: https://www.cancer.org/cancer/breast-cancer/treatment/chemotherapy-for-breast-cancer.html, 2023.
[4] V.T. DeVita, T.S. Lawrence, S.A. Rosenberg, DeVita, Hellman, and Rosenberg's Cancer: Principles & Practice of Oncology, Wolters Kluwer, 2018.
[5] N.L. Henry, P.D. Shah, I. Haider, P.E. Freer, R. Jagsi, M.S. Sabel, 88 - Cancer of the Breast, in: J.E. Niederhuber, J.O. Armitage, M.B. Kastan, J.H. Doroshow, J. E. Tepper (Eds.), Abeloff's Clinical Oncology (Sixth Edition), Elsevier, Philadelphia, 2020, pp. 1560–1603.e12.
[6] L. Poillet-Perez, G. Despouy, R. Delage-Mourroux, M. Boyer-Guittaut, Interplay between ROS and autophagy in cancer cells, from tumor initiation to cancer therapy, Redox Biol. 4 (2015) 184–192.
[7] C.R. Reczek, N.S. Chandel, The two faces of reactive oxygen species in Cancer, Ann. Rev. Cancer Biol. 1 (1) (2017) 79–98.
[8] G.S. Karagiannis, J. Pastoriza, J. Pignatelli, Y. Wang, A.S. Harney, D. Entenberg, et al., Abstract 3963: Neoadjuvant chemotherapy promotes prometastatic changes in the primary breast tumor microenvironment in mice and humans, Cancer Res. 77 (13_Supplement) (2017) 3963.
[9] T.N. Seyfried, L.C. Huysentruyt, On the origin of cancer metastasis, Crit. Rev. Oncog. 18 (1–2) (2013) 43–73.
[10] M. Redza-Dutordoir, D.A. Averill-Bates, Activation of apoptosis signalling pathways by reactive oxygen species, Biochim. Biophys. Acta 1863 (12) (2016) 2977–2992.
[11] L.K. Rausch, N.C. Netzer, J. Hoegel, S. Pramsohler, The Linkage between Breast Cancer, Hypoxia, and Adipose Tissue, Front. Oncol. [Internet] 7 (2017) 211. Available from: http://europepmc.org/abstract/MED/28993797 https://doi.org/10.3389/fonc.2017.00211 https://europepmc.org/articles/PMC5622311 https://europepmc.org/articles/PMC5622311?pdf=render https://www.ncbi.nlm.nih.gov/pmc/articles/PMC5622311/pdf/fonc-07-00211.pdf.
[12] I.I.C. Chio, D.A. Tuveson, ROS in Cancer: the burning question, Trends Mol. Med. 23 (5) (2017) 411–429.
[13] J. Zhang, D. Duan, Z.L. Song, T. Liu, Y. Hou, J. Fang, Small molecules regulating reactive oxygen species homeostasis for cancer therapy, Med. Res. Rev. 41 (1) (2021) 342–394.
[14] J. Prousek, Fenton chemistry in biology and medicine, Pure Appl. Chem. 79 (12) (2007) 2325–2338.
[15] A.V. Snezhkina, A.V. Kudryavtseva, O.L. Kardymon, M.V. Savvateeva, N. V. Melnikova, G.S. Krasnov, A.A. Dmitriev, ROS generation and antioxidant defense systems in normal and malignant cells, Oxidative Med. Cell. Longev. 2019 (2019) 6175804.
[16] D.S. Sigman, D.R. Graham, V. D'Aurora, A.M. Stern, Oxygen-dependent cleavage of DNA by the 1,10-phenanthroline. cuprous complex. Inhibition of *Escherichia coli* DNA polymerase I, J. Biol. Chem. 254 (24) (1979) 12269–12272.
[17] J.J. Rani, S. Roy, Recent development of copper (II) complexes of Polypyridyl ligands in chemotherapy and photodynamic therapy, ChemMedChem. 18 (8) (2023), e202200652.
[18] M. Reina, L.F. Hernández-Ayala, M.E. Bravo-Gómez, V. Gómez, L. Ruiz-Azuara, Second generation of Casiopeinas®: a joint experimental and theoretical study, Inorg. Chim. Acta 517 (2021) 120201.
[19] A. Kellett, M. O'Connor, M. McCann, M. McNamara, P. Lynch, G. Rosair, et al., Bis-phenanthroline copper(II) phthalate complexes are potent in vitro antitumour agents with 'self-activating' metallo-nuclease and DNA binding properties, Dalton Trans. 40 (5) (2011) 1024–1027.
[20] S.G. Davila-Manzanilla, Y. Figueroa-de-Paz, C. Mejia, L. Ruiz-Azuara, Synergistic effects between a copper-based metal Casiopeína III-ia and cisplatin, Eur. J. Med. Chem. 129 (2017) 266–274.
[21] J.R. Valdez-Camacho, Y. Pérez-Salgado, A. Espinoza-Guillén, V. Gómez-Vidales, C. Alberto Tavira-Montalvan, A. Meneses-Acosta, et al., Synthesis, structural characterization and antiproliferative activity on MCF-7 and A549 tumor cell lines

of [cu(N-N)(β3-aminoacidate)]NO3 complexes (Casiopeínas®), Inorg. Chim. Acta 506 (2020) 119542.
[22] S.I. Kirin, C.M. Happel, S. Hrubanova, T. Weyhermüller, C. Klein, N. Metzler-Nolte, Synthesis, structure and comparison of the DNA cleavage ability of metal complexes M(ii)L with the N-(2-ethoxyethanol)-bis(2-picolyl)amine ligand L (M = co, Ni, cu and Zn), Dalton Trans. 8 (2004) 1201–1207.
[23] D.S. Sigman, T.W. Bruice, A. Mazumder, C.L. Sutton, Targeted chemical nucleases, Acc. Chem. Res. 26 (3) (1993) 98–104.
[24] M. Devereux, D. O'Shea, M. O'Connor, H. Grehan, G. Connor, M. McCann, et al., Synthesis, catalase, superoxide dismutase and antitumour activities of copper(II) carboxylate complexes incorporating benzimidazole, 1,10-phenanthroline and bipyridine ligands: X-ray crystal structures of [Cu(BZA)2(bipy)(H2O)], [Cu(SalH)2(BZDH)2] and [cu(CH3COO)2(5,6-DMBZDH)2] (SalH2=salicylic acid; BZAH=benzoic acid; BZDH=benzimidazole and 5,6-DMBZDH=5,6-dimethylbenzimidazole), Polyhedron. 26 (15) (2007) 4073–4084.
[25] M. Devereux, M. McCann, D. O'Shea, M. O'Connor, E. Kiely, V. McKee, et al., Synthesis, Superoxide Dismutase Mimetic and Anticancer Activities of Metal Complexes of 2,2-Dimethylpentanedioic Acid(2dmepdaH2) and 3,3-Dimethylpentanedioic acid(3dmepdaH2): X-Ray Crystal Structures of [Cu(3dmepda)(bipy)]2· 6H2O and [Cu(2dmepda)(bipy)(EtOH)]2· 4EtOH (bipy = 2,2′Bipyridine), Bioinorg. Chem. Appl. 2006 (2006) 080283.
[26] B.S. Creaven, E. Czeglédi, M. Devereux, É.A. Enyedy, A. Foltyn-Arfa Kia, D. Karcz, et al., Biological activity and coordination modes of copper(ii) complexes of Schiff base-derived coumarin ligands, Dalton Trans. 39 (45) (2010) 10854–10865.
[27] P. Nunes, I. Correia, F. Marques, A.P. Matos, M.M.C. Dos Santos, C.G. Azevedo, et al., Copper complexes with 1,10-Phenanthroline derivatives: underlying factors affecting their cytotoxicity, Inorg. Chem. 59 (13) (2020) 9116–9134.
[28] G. Farrugia, R. Balzan, Oxidative stress and programmed cell death in yeast, Front. Oncol. 2 (2012).
[29] D. Hanahan, R.A. Weinberg, Hallmarks of cancer: the next generation, Cell. 144 (5) (2011) 646–674.
[30] B.C. Prager, Q. Xie, S. Bao, J.N. Rich, Cancer stem cells: the architects of the tumor ecosystem, Cell Stem Cell 24 (1) (2019) 41–53.
[31] A. Sharma, J.F. Arambula, S. Koo, R. Kumar, H. Singh, J.L. Sessler, J.S. Kim, Hypoxia-targeted drug delivery, Chem. Soc. Rev. 48 (3) (2019) 771–813.
[32] W.R. Wilson, M.P. Hay, Targeting hypoxia in cancer therapy, Nat. Rev. Cancer 11 (6) (2011) 393–410.
[33] L.L. Parker, S.M. Lacy, L.J. Farrugia, C. Evans, D.J. Robins, C.C. O'Hare, et al., A novel design strategy for stable metal complexes of nitrogen mustards as bioreductive prodrugs, J. Med. Chem. 47 (23) (2004) 5683–5689.
[34] S. Strese, M. Fryknäs, R. Larsson, J. Gullbo, Effects of hypoxia on human cancer cell line chemosensitivity, BMC Cancer 13 (1) (2013) 331.
[35] D. Raydan, I.J. Rivas-Lacre, V. Lubes, V. Landaeta, L. Hernández, Ternary complex formation of the copper (II)-2,2′-Bipyridine system with some amino acids, J. Mol. Liq. 302 (2020) 112595.
[36] L. MacLean, D. Karcz, H. Jenkins, S. McClean, M. Devereux, O. Howe, et al., Copper (II) complexes of coumarin-derived Schiff base ligands: pro- or antioxidant activity in MCF-7 cells? J. Inorg. Biochem. 197 (2019) 110702.
[37] O. Dömötör, N.V. May, G.T. Gál, G. Spengler, A. Dobrova, V.B. Arion, É.A. Enyedy, Solution equilibrium studies on salicylidene aminoguanidine schiff base metal complexes: impact of the hybridization with L-proline on stability, redox activity and cytotoxicity, Molecules 27 (7) (2022).
[38] V.F.S. Pape, R. Palkó, S. Tóth, M.J. Szabó, J. Sessler, G. Dormán, et al., Structure–activity relationships of 8-Hydroxyquinoline-derived Mannich bases with tertiary amines targeting multidrug-resistant Cancer, J. Med. Chem. 65 (11) (2022) 7729–7745.
[39] A. Kellett, O. Howe, M. O'Connor, M. McCann, B.S. Creaven, S. McClean, et al., Radical-induced DNA damage by cytotoxic square-planar copper(II) complexes incorporating o-phthalate and 1,10-phenanthroline or 2,2′-dipyridyl, Free Radic. Biol. Med. 53 (3) (2012) 564–576.
[40] M. Devereux, M. McCann, J.F. Cronin, C. Cardin, A. Todd, Synthesis, X-ray crystal structure and reactivity of the polymeric copper(II) dicarboxylic acid complex {Cu2(η1η1μ2-oda)2(py)4(H2O)2}n(odaH2 = octanedioic acid, py = pyridine), Polyhedron. 15 (5) (1996) 785–791.
[41] J.D. Ranford, P.J. Sadler, D.A. Tocher, Cytotoxicity and antiviral activity of transition-metal salicylato complexes and crystal structure of Bis (diisopropylsalicylato)(1,10-phenanthroline)copper(II), J. Chem. Soc. Dalton Trans. 22 (1993) 3393–3399.
[42] J. Zdravković, D. Poleti, J. Rogan, D.M. Minić, Bis(2,2′-bipyridine)-bis(μ3-phthalato)-dicopper(II) tetrahydrate as molecular sieve with zero-dimensional structure, Polyhedron. 80 (2014) 256–264.
[43] I. Fabian, Hydrolytic reactions of copper(II) bipyridine complexes, Inorg. Chem. 28 (20) (1989) 3805–3807.
[44] H. Sigel, R.B. Martin, Coordinating properties of the amide bond. Stability and structure of metal ion complexes of peptides and related ligands, Chem. Rev. 82 (1982) 385–426.
[45] E. Garribba, G. Micera, The determination of the geometry of cu(II) complexes: an EPR spectroscopy experiment, J. Chem. Educ. 83 (8) (2006) 1229.
[46] E.I. Solomon, J.W. Hare, H.B. Gray, Spectroscopic studies and a structural model for blue copper centers in proteins, Proc. Natl. Acad. Sci. 73 (5) (1976) 1389–1393.
[47] E. Prenesti, P.G. Daniele, S. Berto, S. Toso, Spectrum–structure correlation for visible absorption spectra of copper(II) complexes showing axial co-ordination in aqueous solution, Polyhedron. 25 (15) (2006) 2815–2823.
[48] E. Prenesti, P.G. Daniele, M. Prencipe, G. Ostacoli, Spectrum–structure correlation for visible absorption spectra of copper(II) complexes in aqueous solution, Polyhedron. 18 (25) (1999) 3233–3241.
[49] M. Biagini Cingi, A.M. Manotti Lanfredi, A. Tiripicchio, Camellini M. Tiripicchio, The crystal and molecular structures of magnesium di-o-phthalatocuprate(II) dihydrate and strontium di-o-phthalatocuprate(II) trihydrate, Acta Crystallogr. B 34 (2) (1978) 406–411.
[50] H. Yokoi, A.W. Addison, Spectroscopic and redox properties of pseudotetrahedral copper(II) complexes. Their relation to copper proteins, Inorg. Chem. 16 (1977) 1341–1349.
[51] Z. Derikvand, A. Azadbakht, B. Notash, E. Zamanifar, A new supramolecular coordination compound of mg(II) with chelidamic acid: synthesis, spectroscopic, crystal structures, and thermal analysis, Inorgan. Nano-Metal Chem. 47 (4) (2017) 515–520.
[52] A. Horn, G.L. Parrilha, K.V. Melo, C. Fernandes, M. Horner, Visentin LdC, et al. an Iron-based cytosolic catalase and superoxide dismutase mimic complex, Inorg. Chem. 49 (4) (2010) 1274–1276.
[53] T.P. Ribeiro, C. Fernandes, K.V. Melo, S.S. Ferreira, J.A. Lessa, R.W.A. Franco, et al., Iron, copper, and manganese complexes with in vitro superoxide dismutase and/or catalase activities that keep Saccharomyces cerevisiae cells alive under severe oxidative stress, Free Radic. Biol. Med. 80 (2015) 67–76.
[54] N.D. Amoëdo, J.P. Valencia, M.F. Rodrigues, A. Galina, F.D. Rumjanek, How does the metabolism of tumour cells differ from that of normal cells, Biosci. Rep. 33 (6) (2013), e00080.
[55] K.E. Prosser KE, D. Xie, A. Chu, MacNeil GA, B.R. Varju, R.T. Kadakia, E.L. Que, C. J. Walsby, Copper(II) Pyridyl Aminophenolates: hypoxia-selective, nucleus-targeting Cytotoxins, and magnetic resonance probes, Chem. Eur. J. 27 (2021) 9839–9849.
[56] N.K. Rana, P. Singh, B. Koch, CoCl2 simulated hypoxia induce cell proliferation and alter the expression pattern of hypoxia associated genes involved in angiogenesis and apoptosis, Biol. Res. 52 (1) (2019) 12.
[57] M. Adamaki, A. Georgountzou, M.M. Moschovi, Cancer and the cellular response to hypoxia, Pediat. & Therapeut. 3 (2013) 1–21.
[58] M. Hasanain, R. Sahai, P. Pandey, M. Maheshwari, K. Choyal, D. Gandhi, et al., Microtubule disrupting agent-mediated inhibition of cancer cell growth is associated with blockade of autophagic flux and simultaneous induction of apoptosis, Cell Prolif. 53 (4) (2020), e12749.
[59] A.K. Mukherjee, A.J. Saviola, P.D. Burns, S.P. Mackessy, Apoptosis induction in human breast cancer (MCF-7) cells by a novel venom L-amino acid oxidase (Rusvinoxidase) is independent of its enzymatic activity and is accompanied by caspase-7 activation and reactive oxygen species production, Apoptosis. 20 (10) (2015) 1358–1372.
[60] C. Chu, J. Xu, D. Cheng, X. Li, S. Tong, J. Yan, Q. Li, Anti-proliferative and apoptosis-inducing effects of Camptothecin-20(s)-O-(2-pyrazolyl-1)acetic Ester in human breast tumor MCF-7 cells, Molecules. 19 (4) (2014) 4941–4955.
[61] R. Desai, D.A. East, L. Hardy, D. Faccenda, M. Rigon, J. Crosby, et al., Mitochondria form contact sites with the nucleus to couple prosurvival retrograde response, Sci. Adv. 6 (51) (2020).
[62] R. Kartikeyan, D. Murugan, T. Ajaykamal, M. Varadhan, L. Rangasamy, M. Velusamy, M. Palaniandavar, V. Rajendiran, Mixed ligand copper(II)-diimine complexes of 2-formylpyridine-N^4-phenylthiosemicarbazone: diimine co-ligands tune the *in vitro* nanomolar cytotoxicity, Dalton Trans. 52 (2023) 9148–9169.
[63] Murillo Ml, C. Gaiddon, R. Le Lagadec, Targeting of the intracellular redox balance by metal complexes towards anticancer therapy, Front. Chem. 10 (2022) 967337.
[64] H.M. Irving, M.G. Miles, L.D. Pettit, A study of some problems in determining the stoicheiometric proton dissociation constants of complexes by potentiometric titrations using a glass electrode, Anal. Chim. Acta 38 (1967) 475–488.
[65] É.A. Enyedy, N.V. Nagy, É. Zsigó, C.R. Kowol, V.B. Arion, B.K. Keppler, T. Kiss, Comparative solution equilibrium study of the interactions of copper(II), Iron(II) and zinc(II) with Triapine (3-Aminopyridine-2-carbaldehyde Thiosemicarbazone) and related ligands, Eur. J. Inorg. Chem. 2010 (11) (2010) 1717–1728.
[66] P. Gans, A. Sabatini, A. Vacca, Investigation of equilibria in solution. Determination of equilibrium constants with the HYPERQUAD suite of programs, Talanta. 43 (10) (1996) 1739–1753.
[67] D.J. Leggett, Computational Methods for the Determination of Formation Constants, Springer US, 1985.
[68] A. Rockenbauer, T. Szabó-Plánka, Z. Árkosi, L. Korecz, A two-dimensional (magnetic field and concentration) electron paramagnetic resonance method for analysis of multispecies complex equilibrium systems. information content of EPR spectra, J. Am. Chem. Soc. 123 (31) (2001) 7646–7654.
[69] A. Rockenbauer, L. Korecz, Automatic computer simulations of ESR spectra, Appl. Magn. Reson. 10 (1) (1996) 29–43.
[70] Inc RM, CrystalClear SM. 1.4.0 ed, 2008.
[71] M.C. Burla, R. Caliandro, B. Carrozzini, G.L. Cascarano, C. Cuocci, C. Giacovazzo, et al., Crystal structure determination and refinement via SIR2014, J. Appl. Crystallogr. 48 (1) (2015) 306–309.
[72] University of Gottingen G, SHELXL-2013 Program for Crystal Structure Solution, 2013.

[73] L. Farrugia, WinGX and ORTEP for windows: an update, J. Appl. Crystallogr. 45 (4) (2012) 849–854.
[74] A. Spek, Single-crystal structure validation with the program PLATON, J. Appl. Crystallogr. 36 (1) (2003) 7–13.
[75] C.F. Macrae, P.R. Edgington, P. McCabe, E. Pidcock, G.P. Shields, R. Taylor, et al., Mercury: visualization and analysis of crystal structures, J. Appl. Crystallogr. 39 (3) (2006) 453–457.
[76] F.H. Allen, O. Johnson, G.P. Shields, B.R. Smith, M. Towler, CIF applications. XV. enCIFer: a program for viewing, editing and visualizing CIFs, J. Appl. Crystallogr. 37 (2) (2004) 335–338.
[77] TdP Ribeiro, F.L. Fonseca, M.D.C. de Carvalho, R.M.D.C. Godinho, F.P. de Almeida, T.D. Saint'Pierre, et al., Metal-based superoxide dismutase and catalase mimics reduce oxidative stress biomarkers and extend life span of Saccharomyces cerevisiae, Biochem. J. 474 (2) (2017) 301–315.